

Multiscale approach for variational problem joint diffeomorphic image registration and intensity correction: theory and application*

Peng Chen[†], Ke Chen[‡], Huan Han[§], and Daoping Zhang[¶]

Abstract. Image registration matches the features of two images by minimizing the intensity difference, so that useful and complementary information can be extracted from the mapping. However, in real life problems, images may be affected by the imaging environment, such as varying illumination and noise during the process of imaging acquisition. This may lead to the local intensity distortion, which makes it meaningless to minimize the intensity difference in the traditional registration framework. To address this problem, we propose a variational model for joint image registration and intensity correction. Based on this model, a related greedy matching problem is solved by introducing a multiscale approach for joint image registration and intensity correction. An alternating direction method (ADM) is proposed to solve each multiscale step, and the convergence of the ADM method is proved. For the numerical implementation, a coarse-to-fine strategy is further proposed to accelerate the numerical algorithm, and the convergence of the proposed coarse-to-fine strategy is also established. Some numerical tests are performed to validate the efficiency of the proposed algorithm.

Key words. image registration, diffeomorphism, multiscale, coarse-to-fine, multi-resolution, multigrid

AMS subject classifications. 68U10, 94A08, 65K10, 65M12

1. Introduction. Image registration is to match the features of two images by keeping one image (target image) unchanged and deforming the other image (floating image). By comparing the deformed image with the target image, one can extract useful information from intensity difference. This is a fundamental process for image fusion and medical analysis. For an overview of image registration and related joint problems, one can refer to [1, 3, 5–7, 11, 15, 16, 24, 25, 34] for details.

Without loss of generality, in this paper, we mainly focus on 2D image registration, which is stated in the following way. For some bounded domain $\Omega \subset \mathbb{R}^2$, given two images $T(\mathbf{x}), D(\mathbf{x}) : \mathbf{x} \in \Omega \rightarrow \mathbb{R}$, the goal of image registration is to find a mapping $\varphi(\mathbf{x}) : \mathbf{x} \in \Omega \rightarrow \Omega$ such that

*Submitted to the editors DATE.

Funding: P Chen was supported in part by Natural Science Foundation of Hubei Province of China (No. 2021CFB473); K Chen was supported in part by EPSRC(No. EP/N014499/1); H Han was supported in part by National Natural Science Foundation of China (No.11901443) and Natural Science Foundation of Hubei Province of China (No. 2022CFB379); D Zhang was supported in part by National Natural Science Foundation of China (No. 12201320) and the Fundamental Research Funds for the Central Universities, Nankai University (No. 63221039 and 63231144).

[†]College of Science, China Three Gorges University, Yichang 443002, People's Republic of China (pengchen729@sina.com).

[‡]Department of Mathematics and Statistics, University of Strathclyde, Glasgow, G1 1XH, United Kingdom and Centre for Mathematical Imaging Techniques, University of Liverpool, Liverpool L69 7ZL, United Kingdom (K.Chen@strath.ac.uk).

[§] Corresponding author. Department of Mathematics, Wuhan University of Technology, Wuhan 430070, People's Republic of China (hanhuan11@whut.edu.cn).

[¶]Department of Mathematical Sciences and LPMC, Nankai University, Tianjin 300071, People's Republic of China (daopingzhang@nankai.edu.cn). *All the authors contributed equally to this work.

28 $T \circ \varphi(\cdot)$ looks like $D(\cdot)$ as much as possible. For each $\mathbf{x} \in \Omega$, $\varphi(\mathbf{x})$ can be divided into the
 29 identity part \mathbf{x} and the displacement $\mathbf{u}(\mathbf{x})$, i.e., $\varphi(\mathbf{x}) \triangleq \mathbf{x} + \mathbf{u}(\mathbf{x})$. Based on this assumption,
 30 the mono-modality image registration problem is formulated as follows

$$31 \quad (1.1) \quad \min_{\mathbf{u} \in \mathcal{A}} \lambda S(\mathbf{u}) + \mu R(\mathbf{u}),$$

32 where the fidelity is

$$33 \quad S(\mathbf{u}) = \int_{\Omega} (T(\mathbf{x} + \mathbf{u}(\mathbf{x})) - D(\mathbf{x}))^2 d\mathbf{x},$$

34 $R(\mathbf{u})$ is a regularization to allow plausible solutions, \mathcal{A} is some proper set, and the constants
 35 $\lambda, \mu > 0$ are used to balance the fidelity and regularization. For the multi-modality image
 36 registration [4, 28], the fidelity is

$$37 \quad S(\mathbf{u}) = \int_{\Omega} (f_1(T(\mathbf{x} + \mathbf{u}(\mathbf{x}))) - f_2(D(\mathbf{x})))^2 d\mathbf{x},$$

38 where f_1, f_2 are two intensity transform functions. The problem considered in this paper
 39 lies between these two types of registration problems, because the given images appear in
 40 multi-modality but the modelling must be done in mono-modality.

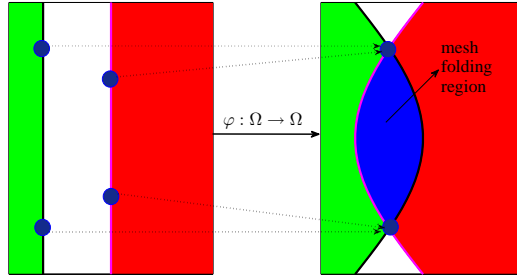


Figure 1. Physical mesh folding caused by the deformation φ

41 Although image registration has achieved enormous success, it is still a challenging task.
 42 There are two main difficulties: (I) physical mesh folding; (II) ill-posedness of greedy match-
 43 ing. As shown in Fig 1, physical mesh folding is a phenomenon that points from different
 44 objects are mixed mutually after doing the transformation. We can find that the essen-
 45 tial reason for mesh folding is the non-bijection of the deformation mapping. Therefore, to
 46 eliminate mesh folding, it is necessary to guarantee that the Jacobian determinant of the
 47 deformation is larger than 0 for each pixel [14, 19, 20]. This is so called ‘orientation-preserving
 48 registration’. Under this framework, some diffeomorphic image registration models have been
 49 proposed [8, 9, 18–20, 22, 27, 30, 31, 36, 39, 40]. Specifically, they can be mainly classified into
 50 three categories: (i) Using quasi conformal/conformal theory [8, 18–20, 22, 27, 30, 31, 36, 39, 40]
 51 to control the Beltrami coefficient; (ii) Constraining the solution to the set which ensures
 52 $\det(\nabla\varphi(\mathbf{x})) > 0$ for each $\mathbf{x} \in \Omega$; (iii) Introducing the stored energy function of an Ogden ma-
 53 terial [9]. For the first choice, Lui [8] introduced the quasi-conformal theory to control the mesh

54 folding. Following this work, several models were proposed to improve the quasi-conformal
 55 model. As a supplement, Zhang and Chen [38] introduced a diffeomorphic image registration
 56 model by controlling the modulus of Beltrami coefficient smaller than 1. Han, Wang and
 57 Zhang also gave a series of 2D/3D diffeomorphic image registration models and algorithms by
 58 restricting \mathbf{u} into the 2D/3D conformal set (Cauchy-Riemann constraint) [18–20, 22]. Partic-
 59 ularly, in [40], Zhang et al. proposed a unifying framework for n -dimensional quasi-conformal
 60 mappings by minimizing the distance between the expected solution and the conformal set.
 61 This framework is essentially equivalent to the relaxed form of the Cauchy-Riemann constrain-
 62 t (Section 2 in [19]) in some sense. For the second choice, Zhang and Chen [42] proposed a
 63 diffeomorphic image registration model by restricting the deformation φ into a set which en-
 64 sures $\det(\nabla\varphi(\mathbf{x})) > 0$ for each $\mathbf{x} \in \Omega$. For the third choice, Debroux, Le Guyader and Vese [9]
 65 established a framework of variational methods and hyperelasticity by viewing the shapes
 66 to be matched as Ogden materials. Though more restrictive compared with quasi-conformal
 67 mappings, the Cauchy-Riemann equation (conformal mapping) [19] is still selected as the con-
 68 straint in this paper by the following reasons: it preserves the topological structure of tissue
 69 and provides a much simpler constraint (linear constraint) for diffeomorphic mappings, which
 70 further makes it possible for the mathematical analysis of the proposed model (i.e., address
 71 the greedy matching [21, 22]).

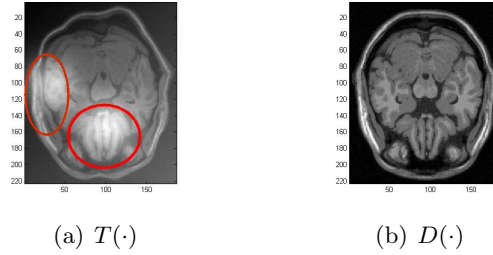


Figure 2. Local varying illumination in MRI image pair

72 Above mentioned works are all based on the assumption that no intensity distortion (i.e.,
 73 illumination and noise) occurs during the process of imaging acquisition. For example, in
 74 Fig 2, the local varying illumination occurs inside the region of the floating image $T(\cdot)$ and
 75 no illumination in the target image $D(\cdot)$. This leads to the intensity distortion for these two
 76 regions. In this case, models such as (1.1) by treating T, D as mono-modal images fail to do the
 77 registration. It is meaningless for latter applications, such as image fusion and image analysis,
 78 even if the sketch of the two objects are exactly matched as a multi-modal problem. Therefore,
 79 it is necessary to introduce some intensity correction steps during or after image registration.
 80 For this purpose, some variational models for joint image registration and intensity correction
 81 are proposed [29, 33]. By introducing the additive and multiplicative bias fields for intensity
 82 correction simultaneously, the relationship between the true image $I^*(\mathbf{x}) = I_c(\mathbf{x})$ and the
 83 obtained image $I(\mathbf{x})$ is formulated as

$$I(\mathbf{x}) = m(\mathbf{x})I^*(\mathbf{x}) + s(\mathbf{x}),$$

85 where $s(\mathbf{x}) : \mathbf{x} \in \Omega \rightarrow \mathbb{R}$ and $m(\mathbf{x}) : \mathbf{x} \in \Omega \rightarrow \mathbb{R}^+$ are additive and multiplicative bias
 86 fields, respectively. Based on the assumption that no bias in target image $D(\cdot)$, Thejani and

87 Chen [33] proposed a model for joint image registration and intensity correction

$$88 \quad (1.2) \quad \min_{\mathbf{u}, m, s} \lambda S_c(\mathbf{u}, m, s) + \mu R(\mathbf{u}, m, s),$$

89 where the fidelity is

$$90 \quad S_c(\mathbf{u}, m, s) = \int_{\Omega} (m(\mathbf{x})D(\mathbf{x}) + s(\mathbf{x}) - T(\mathbf{x} + \mathbf{u}(\mathbf{x})))^2 d\mathbf{x},$$

91 and $R(\mathbf{u}, m, s)$ is a regularization on \mathbf{u}, m and s . Viewing the solution of the variational model
 92 (1.2) as a Nash game equilibrium, a novel numerical algorithm for joint image registration
 93 and intensity correction is also devised in [33]. However, the above mentioned mesh folding
 94 (difficulty I) is not constrained and the game solution is a ‘perturbed solution’, not a minimizer
 95 of the original variational functional. The other works on joint image registration and intensity
 96 correction can be found in [12, 13].

97 The ultimate goal for joint image registration and intensity correction is to find the
 98 minimizer of the cost functional $S_c(\mathbf{u}, m, s)$. However, (1.2) aims to find the minimizer of
 99 $\lambda S_c(\mathbf{u}, m, s) + \mu R(\mathbf{u}, m, s)$. This raises a question of whether or not one can find the glob-
 100 al minimizer of $S_c(\mathbf{u}, m, s)$ on some proper space without any prior estimate for \mathbf{u}, m, s ?
 101 This is so called ‘greedy matching’. Concerning this problem (difficulty II), Han, Wang and
 102 Zhang [21, 22] gave an answer in case of $m(\mathbf{x}) \equiv 1$, $s(\mathbf{x}) \equiv 0$, and T, D having no bias (i.e.,
 103 image registration without intensity correction) by introducing a multiscale approach and
 104 proved the equivalence between the proposed multiscale approach and ‘greedy matching’ with
 105 some suitable parameters. For the general case, to the best of our knowledge, there seems to
 106 have no results. Hence, motivated by [21, 22], in this paper, we aim to extend the work [21]
 107 to the case that m, s belong to some specific Banach spaces. For this purpose, we propose the
 108 following variational model for joint diffeomorphic image registration and intensity correction

$$109 \quad (1.3) \quad \min_{\mathbf{u} \in \mathcal{A}(\Omega) \setminus \mathcal{B}_\varepsilon(\Omega), m \in \mathcal{C}_\Omega, s \in SV_0(\Omega)} J(\mathbf{u}, m, s) := \lambda S_{lc}(\mathbf{u}, m, s) + \mu R(\mathbf{u}, m, s),$$

110 where

$$111 \quad S_{lc}(\mathbf{u}, m, s) = \int_{\Omega} (m(\mathbf{x}) + \ln D(\mathbf{x}) - \ln(T(\mathbf{x} + \mathbf{u}(\mathbf{x})) - s(\mathbf{x})))^2 d\mathbf{x},$$

$$112 \quad R(\mathbf{u}, m, s) = R_1(\mathbf{u}) + R_2(m) + R_3(s),$$

114 and

$$115 \quad R_1(\mathbf{u}) = \int_{\Omega} |\nabla^\alpha \mathbf{u}(\mathbf{x})|^2 d\mathbf{x}, \quad R_2(m) = \int_{\Omega} |\nabla m(\mathbf{x})| d\mathbf{x}, \quad R_3(s) = \int_{\Omega} |\nabla s(\mathbf{x})| d\mathbf{x}.$$

117 Note that here and in what follows, we assume that two images T, D map Ω onto the interval
 118 $[\kappa, \bar{M}] \subset \mathbb{R}^+$ for some $\bar{M} > \kappa > 0$. In addition, for the purpose of eliminating mesh folding,
 119 \mathbf{u} is constrained into the set $\mathcal{A}(\Omega) \setminus \mathcal{B}_\varepsilon(\Omega)$, where $\mathcal{A}(\Omega)$ and $\mathcal{B}_\varepsilon(\Omega)$ are defined by

$$120 \quad (1.4) \quad \mathcal{A}(\Omega) = \left\{ \mathbf{u} = (u_1, u_2)^T \in [H_0^\alpha(\Omega)]^2 : \frac{\partial u_1}{\partial x_1} = \frac{\partial u_2}{\partial x_2}, \frac{\partial u_1}{\partial x_2} = -\frac{\partial u_2}{\partial x_1} \right\}$$

121

122 and

$$123 \quad (1.5) \quad \mathcal{B}_\varepsilon(\Omega) = \{\mathbf{u} = (u_1, u_2)^T \in \mathcal{A}(\Omega) : \det(\nabla(\mathbf{x} + \mathbf{u}(\mathbf{x}))) < \varepsilon\},$$

125 for some given fractional-order α ($\alpha > 2$), small $\varepsilon > 0$, and $H_0^\alpha(\Omega)$ is fractional-order Sobolev space [17]. To control the intensity bias in practice, the multiplicative bias field m is constrained into the set

$$128 \quad (1.6) \quad \mathcal{C}_\Omega = \{m \in BV_0(\Omega) : K_1 \leq m \leq K_2\},$$

130 for some given K_1, K_2 , and the additive bias field s is constrained into the set

$$131 \quad SV_0(\Omega) = \{s \in BV_0(\Omega) : s(\mathbf{x}) < \kappa - \kappa_0 \text{ for } \forall \mathbf{x} \in \Omega\},$$

133 for some $\kappa > \kappa_0 > 0$ to ensure that $\ln(T(\mathbf{x} + \mathbf{u}(\mathbf{x})) - s(\mathbf{x}))$ is well-defined. Here, $BV_0(\Omega) =$
134 $\{m \in BV(\Omega) : m(\mathbf{x})|_{\mathbf{x} \in \partial\Omega} = 0\}$ and the space $BV(\Omega)$ is defined in [32].

135 *Remark 1.1.* In the proposed model (1.3), the fractional-order α is set to be greater than
136 2 to ensure that the first-order derivatives in $\mathcal{A}(\Omega)$ are well defined ($H_0^\alpha(\Omega) \hookrightarrow C^1(\Omega)$ for
137 $\alpha > 2$ (Theorem 4.58 in [10])). In addition, by letting $m(\mathbf{x}) \equiv 1$ and $s(\mathbf{x}) \equiv 0$, one can notice
138 that the model (1.2) is reduced to the model (1.1), which means that the model (1.2) is much
139 more general than the model (1.1).

140 *Remark 1.2.* By setting $m(\mathbf{x}) = \ln \bar{m}(\mathbf{x})$ for some positive function $\bar{m}(\mathbf{x})$, $S_{lc}(\mathbf{u}, m, s)$ from
141 (1.2) becomes

$$142 \quad (1.7) \quad S_{lc}(\mathbf{u}, m, s) = \int_{\Omega} \left(\ln \frac{T(\mathbf{x} + \mathbf{u}(\mathbf{x})) - s(\mathbf{x})}{\bar{m}(\mathbf{x})D(\mathbf{x})} \right)^2 dx.$$

143 That is, minimizing $S_{lc}(\mathbf{u}, m, s)$ in (1.3) is equivalent to minimizing $S_c(\mathbf{u}, m, s)$ in (1.2). Using
144 (1.7) as the data fidelity for (1.3) has two advantages: (i) transforming the multiplicative
145 bias field into the additive bias field; (ii) eliminating the positive constraint $m(\mathbf{x}) > 0$ in
146 the definition of $S_c(\mathbf{u}, m, s)$. In addition, by using $S_{lc}(\mathbf{u}, m, s)$ as the fidelity data, the final
147 matched image for (1.3) should be calculated as $T_c(\cdot) = \frac{T(+\mathbf{u}(\cdot)) - s(\cdot)}{e^{m(\cdot)}}$.

148 *Remark 1.3.* Similar to the model (1.2), the fidelity in (1.3) is formulated based on the
149 assumption that the target image $D(\cdot)$ has no bias. For the situation where $T(\cdot)$ and $D(\cdot)$
150 are both affected by bias, two different biases (i.e., m_T, s_T and m_D, s_D) are necessary to
151 be introduced to construct a Bi-bias fidelity $S_{lc}(\mathbf{u}, m_T, s_T, m_D, s_D)$. This situation will be
152 considered in our forthcoming work.

153 Further, based on the model (1.3), in this paper, we propose a multiscale approach for
154 joint image registration and intensity correction, which aims to find the global minimizer of
155 $S_{lc}(\mathbf{u}, m, s)$ on $\mathcal{A} \times \mathcal{C}_\Omega \times SV_0(\Omega)$ for some given K_1, K_2 (see Section 2 for details), namely,
156 $\inf_{(\mathbf{u}, m, s) \in \mathcal{A} \times \mathcal{C}_\Omega \times SV_0(\Omega)} S_{lc}(\mathbf{u}, m, s)$. This is so called ‘greedy problem’ for joint diffeomorphic
157 image registration and intensity correction, which searches for the global minimizer of the
158 similarity $S_{lc}(\mathbf{u}, m, s)$ by placing the regularization into the constraint set $\mathcal{A} \times \mathcal{C}_\Omega \times SV_0(\Omega)$.
159 The main contributions of the proposed multiscale approach contain three aspects:

- 160 • Propose a novel model for joint image registration and intensity correction;
- 161 • Address the greedy problem for joint image registration and intensity correction;
- 162 • Eliminate the intensity inhomogeneity by removing the bias.

163 The rest of this paper is organized as follows. In Section 2, we propose a multiscale
 164 approach for (1.3) to address the ‘greedy problem’. In Section 3, an ADM method to solve
 165 the joint model for each scale is discussed and the convergence is also proved under some
 166 suitable assumptions. In Section 4, we propose a coarse-to-fine strategy for the multiscale
 167 approach to further accelerate the algorithm. In Section 5, some applications of the proposed
 168 multiscale approach are performed. Finally, we conclude our work and outline some problems
 169 for the future research in Section 7.

170 **2. Multiscale approach based on the model (1.3) and related greedy problem.** Mesh
 171 folding may occur in the large deformation registration. To control the mesh folding in
 172 the large deformation registration, one can decompose the large deformation $\tilde{\varphi}_n$ into the
 173 composition of some small deformations $\varphi_i (i = 0, 1, 2, \dots, n)$ [9, 21, 22], where φ_i are the
 174 deformation induced by different scales (different variational problems). This is the reason
 175 where the ‘multiscale’ comes from. Furthermore, we have two choices for this decomposition:
 176 (i) minimizing the functional that contains fidelity and regularization by keeping parameters
 177 unchanged for different scales [9]; (ii) minimizing the fidelity by setting some specific varying
 178 parameters for different scales [21, 22]. Motivated by [21, 22], we propose a multiscale approach
 179 based on the model (1.3) to give an answer to the question of whether or not one can find the
 180 global minimizer of $S_{lc}(\mathbf{u}, m, s)$ on $\mathcal{L}(\Omega) = \mathcal{A}(\Omega) \times \mathcal{C}_\Omega \times SV_0(\Omega)$. The multiscale approach is
 181 divided into the following n steps:

182 **Step 0.** Searching for the solution of the following variational problem:

$$183 \quad (2.1) \quad (\mathbf{u}_0, m_0, s_0) \in \underset{(\mathbf{u}, m, s) \in \mathcal{L}_{\varepsilon_0}(\Omega)}{\arg \min} J_0(\mathbf{u}, m, s),$$

184 where $J_0(\mathbf{u}, m, s) = \lambda_0 \int_\Omega (m(\mathbf{x}) + \ln D(\mathbf{x}) - \ln(T(\mathbf{x} + \mathbf{u}(\mathbf{x})) - s(\mathbf{x})))^2 d\mathbf{x} + \mu R(\mathbf{u}, m, s)$, $\mathcal{L}_{\varepsilon_0}(\Omega) =$
 185 $(\mathcal{A}(\Omega) \setminus \mathcal{B}_{\varepsilon_0}(\Omega)) \times \mathcal{C}_\Omega \times SV_0(\Omega)$, and $\varepsilon_0 > 0$. Define $\tilde{\varphi}_0(\mathbf{x}) = \varphi_0(\mathbf{x}) = \mathbf{x} + \mathbf{u}_0(\mathbf{x})$.

186 **Step 1.** Searching for the solution of the following variational problem:

$$187 \quad (\mathbf{u}_1, \delta m_1, \delta s_1) \in \underset{(\mathbf{u}, m_0 + m, s_0 + s) \in \mathcal{L}_{\varepsilon_1}(\Omega)}{\arg \min} J_1(\mathbf{u}, m, s),$$

188 where $J_1(\mathbf{u}, m, s) = \lambda_1 \int_\Omega (m_0(\mathbf{x}) + m(\mathbf{x}) + \ln D(\mathbf{x}) - \ln(T \circ \tilde{\varphi}_0(\mathbf{x} + \mathbf{u}(\mathbf{x})) - s_0(\mathbf{x}) - s(\mathbf{x})))^2 d\mathbf{x} +$
 189 $\mu R(\mathbf{u}, m, s)$, $\mathcal{L}_{\varepsilon_1}(\Omega) = (\mathcal{A}(\Omega) \setminus \mathcal{B}_{\varepsilon_1}(\Omega)) \times \mathcal{C}_\Omega \times SV_0(\Omega)$ and $\varepsilon_1 > 0$. Define $\varphi_1(\mathbf{x}) = \mathbf{x} + \mathbf{u}_1(\mathbf{x})$,
 190 $\tilde{\varphi}_1(\mathbf{x}) = \tilde{\varphi}_0 \circ \varphi_1(\mathbf{x})$, $m_1(\mathbf{x}) = m_0(\mathbf{x}) + \delta m_1(\mathbf{x})$ and $s_1(\mathbf{x}) = s_0(\mathbf{x}) + \delta s_1(\mathbf{x})$.

191 \vdots

192 **Step n.** By induction, for $n \geq 1$, searching for the solution of the following variational
 193 problem:

$$194 \quad (2.2) \quad (\mathbf{u}_n, \delta m_n, \delta s_n) \in \underset{(\mathbf{u}, m_{n-1} + m, s_{n-1} + s) \in \mathcal{L}_{\varepsilon_n}(\Omega)}{\arg \min} J_n(\mathbf{u}, m, s),$$

195 where $J_n(\mathbf{u}, m, s) = \lambda_n \int_{\Omega} (m_{n-1}(\mathbf{x}) + m(\mathbf{x}) + \ln D(\mathbf{x}) - \ln(T \circ \tilde{\varphi}_{n-1}(\mathbf{x} + \mathbf{u}(\mathbf{x})) - s(\mathbf{x})))^2 d\mathbf{x} + \mu R(\mathbf{u}, m, s)$, $\mathcal{L}_{\varepsilon_n}(\Omega) = (\mathcal{A}(\Omega) \setminus \mathcal{B}_{\varepsilon_n}(\Omega)) \times \mathcal{C}_{\Omega} \times SV_0(\Omega)$ and $\varepsilon_n > 0$. Define $\varphi_n(\mathbf{x}) =$
 196 $\mathbf{x} + \mathbf{u}_n(\mathbf{x})$, $\tilde{\varphi}_n(\mathbf{x}) = \tilde{\varphi}_{n-1} \circ \varphi_n(\mathbf{x})$, $m_n(\mathbf{x}) = m_{n-1}(\mathbf{x}) + \delta m_n(\mathbf{x})$ and $s_n(\mathbf{x}) = s_{n-1}(\mathbf{x}) + \delta s_n(\mathbf{x})$.
 197
 198

199 Note that here the final deformation is $\tilde{\varphi}_n(\mathbf{x}) = \varphi_0 \circ \varphi_1 \circ \cdots \circ \varphi_n(\mathbf{x})$. This implies, when
 200 n is large enough (In practice, $n = 5$ is usually enough to achieve a convergent result), the
 201 multiscale approach (2.1)-(2.2) can simulate a large deformation well even if $\varphi_i (i = 0, 1, \dots, n)$
 202 is a small deformation. In addition, there are two key parameters λ_n, ε_n in the multiscale
 203 approach (2.1)-(2.2). These parameters determine whether or not one can find the global
 204 minimizer of $S_{lc}(\mathbf{u}, m, s)$ on $\mathcal{L}(\Omega)$. In practice, λ_n and ε_n are set to be large numbers and
 205 small positive numbers, respectively. However, this is not enough. For example, similar to
 206 the idea in [9], by keeping λ_n as a large constant, one can only achieve the minimizer of
 207 $J(\mathbf{u}, m, s)$. In addition, the ratio λ_n of fidelity may change with scale number n . That is,
 208 the final deformation is the composition of the deformations of different variational problems.
 209 This is the outcome where the multiscale comes from.

210 In order to use the multiscale approach (2.1)-(2.2) to solve the greedy matching problem
 211 well, we shall give a more precise condition shortly (i.e., λ_n and ε_n satisfy the convergence
 212 condition in Theorem 2.6).

213 Before that, concerning the existence of the solution for (2.2), we have the following result.
 214

215 **Theorem 2.1.** *Assume that $\max_{\mathbf{x} \in \Omega} |T(\mathbf{x})| < M < +\infty$, $\max_{\mathbf{x} \in \Omega} |D(\mathbf{x})| < M < +\infty$, and $\Delta_T \triangleq$
 216 $\{\mathbf{x} : T(\mathbf{x}) \text{ is discontinuous at } \mathbf{x}\}$ is a zero measure set, then there exists at least one solution
 217 for (2.2).*

218 *Proof.* By selecting a minimizing sequence $\{(\mathbf{u}^k, \delta m^k, \delta s^k)\}$ of the functional $J_n(\mathbf{u}, \delta m, \delta s)$,
 219 due to $J_n(\mathbf{u}, \delta m, \delta s) \leq J_n(\mathbf{0}, 0, 0)$, one can conclude that \mathbf{u}^k , δm^k and δs^k are bounded on
 220 $[H^\alpha(\Omega)]^2$, $BV_0(\Omega)$ and $BV_0(\Omega)$, respectively.

221 Firstly, by the compactness of $H^\alpha(\Omega)$, there exists a subsequence of \mathbf{u}^k which are still
 222 labelled by k and $\mathbf{u} \in [H^\alpha(\Omega)]^2$ such that \mathbf{u}^k weakly converges to \mathbf{u} with $R_1(\mathbf{u}) \leq \lim_{k \rightarrow \infty}$
 223 $\inf R_1(\mathbf{u}^k)$. By the compact embedding theorem (Theorem 4.58 in [10]), we know that $H_0^\alpha(\Omega)$
 224 $\hookrightarrow C^1(\Omega)$. Namely, there exists a subsequence of \mathbf{u}^k which are still labelled by k and $\bar{\mathbf{u}} \in$
 225 $[C^1(\Omega)]^2$ such that \mathbf{u}^k converges to $\bar{\mathbf{u}}$ in $[C^1(\Omega)]^2$. Moreover, by the uniqueness of the limit,
 226 we get $\bar{\mathbf{u}} = \mathbf{u}$. That is, $\mathbf{u}^k \xrightarrow{k} \mathbf{u}$ in $[C^1(\Omega)]^2$. Therefore, we conclude $\mathbf{u} \in \mathcal{A}(\Omega) \setminus \mathcal{B}_{\varepsilon_n}(\Omega)$.

227 Secondly, by the compactness on $BV(\Omega)$, there exists a subsequence of δm^k which are still
 228 labelled by k and $\delta m \in BV(\Omega)$ such that δm^k weakly converges to δm with

$$229 \quad (2.3) \quad \|\delta m^k - \delta m\|_{L^1(\Omega)} \xrightarrow{k} 0 \text{ and } \int_{\Omega} \nabla \delta m^k \cdot \varphi d\mathbf{x} \xrightarrow{k} \int_{\Omega} \nabla \delta m \cdot \varphi d\mathbf{x}, \quad \forall \varphi \in C_0^\infty(\Omega),$$

231 where the first equation in (2.3) implies $m_{n-1} + \delta m \in C_\Omega$ and the second equation in (2.3)
 232 implies $R_2(m^k) \xrightarrow{k} R_2(m)$.

233 Similarly to the analysis on δm^k , one can again conclude that there exists a subsequence

234 of δs^k which are still labelled by k and $\delta s \in BV(\Omega)$ such that δs^k weakly converges to δs with

$$235 \quad (2.4) \quad \|\delta s^k - \delta s\|_{L^1(\Omega)} \xrightarrow{k} 0 \text{ and } \int_{\Omega} \nabla \delta s^k \cdot \varphi d\mathbf{x} \xrightarrow{k} \int_{\Omega} \nabla \delta s \cdot \varphi d\mathbf{x}, \quad \forall \varphi \in C_0^\infty(\Omega),$$

237 where the first equation in (2.4) implies $s_{n-1} + \delta m \in SV_0(\Omega)$ and the second equation in (2.4)
238 implies $R_3(\delta s^k) \xrightarrow{k} R_3(\delta s)$.

239 Finally, by $\|\mathbf{u}^k - \mathbf{u}\|_{[C^1(\Omega)]^2} \xrightarrow{k} 0$, $\|\delta m^k - \delta m\|_{L^1(\Omega)} \xrightarrow{k} 0$ and $\|\delta s^k - \delta s\|_{L^1(\Omega)} \xrightarrow{k} 0$, we
240 obtain $\int_{\Omega} (m_{n-1}(\mathbf{x}) + \delta m^k(\mathbf{x}) + \ln D(\mathbf{x}) - \ln(T \circ \tilde{\varphi}_{n-1}(\mathbf{x} + \mathbf{u}^k(\mathbf{x})) - s_{n-1}(\mathbf{x}) - \delta s^k(\mathbf{x})))^2 d\mathbf{x} \xrightarrow{k}$
241 $\int_{\Omega} (m_{n-1}(\mathbf{x}) + \delta m(\mathbf{x}) + \ln D(\mathbf{x}) - \ln(T \circ \tilde{\varphi}_{n-1}(\mathbf{x} + \mathbf{u}(\mathbf{x})) - s_{n-1}(\mathbf{x}) - \delta s(\mathbf{x})))^2 d\mathbf{x}$. Note that here
242 we use $\tilde{\varphi}_{n-1} \in [C^1(\Omega)]^2$, which implies that $T \circ \tilde{\varphi}_{n-1}(\cdot)$ is continuous except on some zero
243 measure set. Therefore, $J_n(\mathbf{u}, \delta m, \delta s) \leq \liminf_{k \rightarrow \infty} J_n(\mathbf{u}^k, \delta m^k, \delta s^k)$, which ensures the existence
244 of solution for (2.2). ■

245 Then recall some important lemmas in [21], which are necessary for the proof of the
246 convergence of the multiscale approach (2.1)-(2.2).

247 **Lemma 2.2.** *Assume $\mathbf{f}, \mathbf{g} : \Omega \rightarrow \Omega$, $\mathcal{W}(\mathbf{f}) = \mathbf{f} - \mathbf{I}$ and \mathbf{I} is the identity mapping, then there*
248 *holds*

- 249 (i) *If $\mathcal{W}(\mathbf{f}) \in \mathcal{A}(\Omega) \setminus \mathcal{B}_{\varepsilon_1}(\Omega)$, $\mathcal{W}(\mathbf{g}) \in \mathcal{A}(\Omega) \setminus \mathcal{B}_{\varepsilon_2}(\Omega)$, then $\mathcal{W}(\mathbf{f} \circ \mathbf{g}) \in \mathcal{A}(\Omega) \setminus \mathcal{B}_{\varepsilon_1 \varepsilon_2}(\Omega)$.*
- 250 (ii) *If $\mathcal{W}(\mathbf{f}) \in \mathcal{A}(\Omega) \setminus \mathcal{B}_{\varepsilon}(\Omega)$, then there exists $\mathbf{g} = \mathbf{f}^{-1} \in \mathcal{A}(\Omega)$.*
- 251 (iii) *If $\mathcal{W}(\mathbf{g}) \in \mathcal{A}(\Omega) \setminus \mathcal{B}_{\varepsilon}(\Omega)$, then there exists a constant C_1 such that $\int_{\Omega} \mathbf{f}(\mathbf{g}(\mathbf{x})) d\mathbf{x} \leq$*
252 *$C_1 R_1(\mathbf{g}^{-1}) \int_{\Omega} \mathbf{f}(\mathbf{y}) d\mathbf{y}$.*

253 **Remark 2.3.** Recall that the deformation $\varphi : \Omega \rightarrow \Omega$ is defined to be the sum of the
254 identity map and displacement $\mathbf{u} : \Omega \rightarrow \mathbb{R}$, namely, $\varphi(\mathbf{x}) = \mathbf{x} + \mathbf{u}(\mathbf{x})$. Here, the operator \mathcal{W}
255 is introduced to distinguish the deformation and displacement and simplify the description in
256 the proof of Theorem 2.6. In fact, $\mathcal{W}(\varphi) = \mathbf{u}$.

257 **Lemma 2.4.** *Assume $\mathbf{p}(\mathbf{x}) = \mathbf{x} + \mathbf{u}(\mathbf{x})$ and $\mathcal{W}(\mathbf{q}) \in \mathcal{A}(\Omega) \setminus \mathcal{B}_{\varepsilon}(\Omega)$, then there exists a*
258 *constant C_2 such that $R_1(\mathcal{W}(\mathbf{p} \circ \mathbf{q})) = 2(R_1(\mathcal{W}(\mathbf{q})) + C_2 R_1(\mathbf{q}^{-1}) R_1(\mathcal{W}(\mathbf{p})))$.*

259 **Lemma 2.5.** *Assume $\varphi(\mathbf{x}) = \mathbf{x} + \mathbf{u}(\mathbf{x})$, $\mathbf{g}(\mathbf{x}) = \varphi^{-1}(\mathbf{x}) = \mathbf{x} + \mathbf{v}(\mathbf{x})$, and $\mathbf{u}, \mathbf{v} \in \mathcal{A}(\Omega) \setminus \mathcal{B}_{\varepsilon}(\Omega)$,*
260 *then there exists a constant C_3 such that $R_1(\mathbf{u}) = \int_{\Omega} \|\nabla^\alpha \mathbf{u}(\mathbf{x})\|^2 d\mathbf{x} \leq C_3 R_1(\mathbf{g}) R_1(\mathcal{W}(\mathbf{g}))$.*

261 Based on these lemmas, we are now ready to give the result on the convergence of the
262 multiscale approach (2.1)-(2.2).

263 By setting $m \equiv 0$, $s \equiv 0$ and $\mathbf{u} \equiv \mathbf{0}$, it follows from $J_n(\mathbf{u}_n, \delta m_n, \delta s_n) \leq J_n(\mathbf{0}, 0, 0)$ in (2.2)
264 that

$$265 \quad \lambda_n S_{lc}^n(\mathbf{u}_n, m_n, s_n) + \mu R(\mathbf{u}_n, \delta m_n, \delta s_n) \leq \lambda_n S_{lc}^{n-1}(\mathbf{u}_{n-1}, m_{n-1}, s_{n-1}),$$

266 where

$$267 \quad S_{lc}^n(\mathbf{u}_n, m_n, s_n) = \int_{\Omega} (m_n(\mathbf{x}) + \ln D(\mathbf{x}) - \ln(T \circ \tilde{\varphi}_n(\mathbf{x}) - s_n(\mathbf{x})))^2 d\mathbf{x},$$

268 and $R(\mathbf{0}, 0, 0) = 0$. Hence, $S_{lc}^n(\mathbf{u}_n, m_n, s_n)$ is a decreasing sequence with a lower bound, whose
 269 limit is defined by

$$270 \quad (2.5) \quad \delta = \lim_{n \rightarrow +\infty} S_{lc}^n(\mathbf{u}_n, m_n, s_n).$$

271 Define

$$272 \quad (2.6) \quad \phi = \inf_{(\mathbf{u}, m, s) \in \mathcal{L}(\Omega)} \int_{\Omega} (m(\mathbf{x}) + \ln D(\mathbf{x}) - \ln(T(\mathbf{x} + \mathbf{u}(\mathbf{x})) - s(\mathbf{x})))^2 dx.$$

273 By proving $\delta = \phi$ under some suitable assumptions, we can give an answer to the problem
 274 of whether or not one can find the global minimizer of $S_{lc}(\mathbf{u}, m, s)$ on a proper set $\mathcal{L}(\Omega) =$
 275 $\mathcal{A}(\Omega) \times \mathcal{C}_{\Omega} \times SV_0(\Omega)$. Note that (1.4)-(1.6) imply $\mathcal{A}(\Omega) \subseteq [H_0^{\alpha}(\Omega)]^2$, $\mathcal{C}_{\Omega} \subseteq BV(\Omega)$, and
 276 $SV_0(\Omega) \subseteq BV(\Omega)$, which ensures that the greedy matching problem (2.6) is well regularized.

277 **Theorem 2.6.** *Let $\varphi_n, \tilde{\varphi}_n, m_n$ and s_n be induced by the multiscale approach (2.1)-(2.2),*
 278 *and assume that B, M and λ_n are three positive numbers satisfying $\lim_{n \rightarrow +\infty} \frac{B^{4n-3}M^{4n}}{\lambda_n} = 0$ and*
 279 *$\lim_{n \rightarrow +\infty} \varepsilon_n = 0$, where B is a positive number depending on Ω and M is a positive number*
 280 *depending on $\mathbf{u}_0, \delta m_0, \delta s_0, \Omega, \alpha$ and ϕ , respectively. Then there holds $\phi = \delta$.*

281 *Proof.* It is obvious that $\delta \geq \phi$. To show $\delta \leq \phi$, we use the contradiction.

282 Assume $\delta > \phi$, then there exists a $C_1 \in (0, 1)$ such that $\phi < C_1\delta < \delta$. By the definition of
 283 ϕ , there exists $\bar{\varphi}(\mathbf{x}) = \mathbf{x} + \bar{\mathbf{u}}(\mathbf{x}) \in \mathcal{A}(\Omega)$, $\bar{m} \in \mathcal{C}_{\Omega}$ and $\bar{s} \in SV_0(\Omega)$ such that

$$284 \quad (2.7) \quad \|\bar{m} + \ln D - \ln(T \circ \bar{\varphi} - \bar{s})\|_{L^2(\Omega)}^2 < C_1\delta.$$

285 Setting $\varphi = \tilde{\varphi}_{n-1}^{-1} \circ \bar{\varphi}$, $m = \bar{m} - m_{n-1}$, $s = \bar{s} - s_{n-1}$, by Lemma 2.2, we obtain $\varphi \in \mathcal{A}(\Omega)$,
 286 $m_{n-1} + m \in \mathcal{C}_{\Omega}$ and $s_{n-1} + s \in SV_0(\Omega)$. By (2.2), (2.5) and (2.7), we have

$$287 \quad (2.8) \quad \begin{aligned} & \lambda_n \int_{\Omega} (\tilde{m}_n(\mathbf{x}) + \ln D(\mathbf{x}) - \ln(T \circ \tilde{\varphi}_n(\mathbf{x}) - \tilde{s}_n(\mathbf{x})))^2 dx + \mu R(\mathbf{u}_n, \delta m_n, \delta s_n) \\ & \leq \lambda_n \|\bar{m} + \ln D - \ln(T \circ \varphi - \bar{s})\|_{L^2(\Omega)}^2 + \mu R(\mathcal{W}(\tilde{\varphi}_{n-1}^{-1} \circ \bar{\varphi}), \bar{m} - m_{n-1}, \bar{s} - s_{n-1}) \\ & \leq \lambda_n C_1 \delta + \mu R(\mathcal{W}(\tilde{\varphi}_{n-1}^{-1} \circ \bar{\varphi}), \bar{m} - m_{n-1}, \bar{s} - s_{n-1}). \end{aligned}$$

288 Then by (2.8), we further have

$$289 \quad (2.9) \quad \lambda_n(1 - C_1)\delta + \mu R(\mathbf{u}_n, \delta m_n, \delta s_n) \leq \mu R(\mathcal{W}(\tilde{\varphi}_{n-1}^{-1} \circ \bar{\varphi}), \bar{m} - m_{n-1}, \bar{s} - s_{n-1})$$

290 and

$$291 \quad (2.10) \quad R(\mathbf{u}_n, \delta m_n, \delta s_n) \leq R(\mathcal{W}(\tilde{\varphi}_{n-1}^{-1} \circ \bar{\varphi}), \bar{m} - m_{n-1}, \bar{s} - s_{n-1}).$$

292 Recall $R(\mathbf{u}, m, s) = R_1(\mathbf{u}) + R_2(m) + R_3(s)$. Based on the inequality $|a + b| \leq |a| + |b|$
 293 and the fact $m_{n-1} = m_{n-2} + \delta m_{n-1}$, $s_{n-1} = s_{n-2} + \delta s_{n-1}$, we obtain

$$294 \quad (2.11) \quad R_2(\bar{m} - m_{n-1}) \leq R_2(\bar{m} - m_{n-2}) + R_2(\delta m_{n-1}), \quad R_3(\bar{s} - s_{n-1}) \leq R_3(\bar{s} - s_{n-2}) + R_3(\delta s_{n-1}).$$

295 To estimate $R_1(\mathcal{W}(\tilde{\varphi}_{n-1}^{-1} \circ \bar{\varphi}))$, by Lemma 2.4, we obtain

$$296 \quad (2.12) \quad R_1(\mathcal{W}(\tilde{\varphi}_{n-1}^{-1} \circ \bar{\varphi})) \leq 2R_1(\mathcal{W}(\tilde{\varphi}_{n-2}^{-1} \circ \bar{\varphi})) + 2CR_1((\tilde{\varphi}_{n-2}^{-1} \circ \bar{\varphi})^{-1})R_1(\mathcal{W}(\varphi_{n-1}^{-1})),$$

297 where we use the formula $\tilde{\varphi}_{n-1}^{-1} \circ \bar{\varphi} = \varphi_{n-1}^{-1} \circ \tilde{\varphi}_{n-2}^{-1} \circ \bar{\varphi} = \varphi_{n-1}^{-1} \circ (\tilde{\varphi}_{n-2}^{-1} \circ \bar{\varphi})$. Concerning the
298 estimates on $R_1((\tilde{\varphi}_{n-2}^{-1} \circ \bar{\varphi})^{-1})$ and $R_1(\mathcal{W}(\varphi_{n-1}^{-1}))$, we have

$$\begin{aligned} & R_1((\tilde{\varphi}_{n-2}^{-1} \circ \bar{\varphi})^{-1}) \leq 2R_1(\mathbf{x}) + 2R_1(\mathcal{W}((\tilde{\varphi}_{n-2}^{-1} \circ \bar{\varphi})^{-1})) \\ & \leq \tilde{c}_1 R_1(\tilde{\varphi}_{n-2}^{-1} \circ \bar{\varphi}) R_1(\mathcal{W}((\tilde{\varphi}_{n-2}^{-1} \circ \bar{\varphi}))) + \tilde{c}_2 \\ 299 \quad (2.13) \quad & \leq \tilde{c}_3 R_1^2(\mathcal{W}(\tilde{\varphi}_{n-2}^{-1} \circ \bar{\varphi})) + \tilde{c}_4 R_1(\mathcal{W}(\tilde{\varphi}_{n-2}^{-1} \circ \bar{\varphi})) + \tilde{c}_5 \\ & \leq B_1 \mathcal{M}^2((R_1(\mathcal{W}(\tilde{\varphi}_{n-2}^{-1} \circ \bar{\varphi}))) \end{aligned}$$

300 and

$$\begin{aligned} & R_1(\mathcal{W}(\varphi_{n-1}^{-1})) \leq CR_1(\mathcal{W}(\varphi_{n-1}))R_1(\varphi_{n-1}) \\ 301 \quad (2.14) \quad & \leq CR_1(\mathcal{W}(\varphi_{n-1}))(\bar{C} + R_1(\mathcal{W}(\varphi_{n-1}))) \\ & \leq B_0 \mathcal{M}^2(R_1(\mathcal{W}(\varphi_{n-1}))), \end{aligned}$$

302 where for any $\xi \geq 0$,

$$303 \quad \mathcal{M}(\xi) = \begin{cases} 1, & 0 \leq \xi \leq 1, \\ \xi, & \xi > 1. \end{cases}$$

304 The first and third inequalities in (2.13) are based on the fact that $\mathbf{f}(\mathbf{x}) = \mathbf{x} + \mathcal{W}(\mathbf{f})$ for any
305 deformation \mathbf{f} , and the second inequality in (2.13) is based on the conclusion $R_1(\mathcal{W}(\mathbf{g}^{-1})) \leq$
306 $CR_1(\mathbf{g})R_1(\mathcal{W}(\mathbf{g}))$ in Lemma 2.5. Hence, by (2.12), (2.13) and (2.14), we get

$$307 \quad (2.15) \quad R_1(\mathcal{W}(\tilde{\varphi}_{n-1}^{-1} \circ \bar{\varphi})) \leq 2R_1(\mathcal{W}(\tilde{\varphi}_{n-2}^{-1} \circ \bar{\varphi})) + B\mathcal{M}^2(R_1(\mathcal{W}(\varphi_{n-1})))\mathcal{M}^2(R_1(\mathcal{W}(\tilde{\varphi}_{n-2}^{-1} \circ \bar{\varphi}))).$$

308 Furthermore, by (2.10), (2.11) and (2.15), we have

$$\begin{aligned} & (2.16) \quad R(\mathcal{W}(\tilde{\varphi}_{n-1}^{-1} \circ \bar{\varphi}), \bar{m} - m_{n-1}, \bar{s} - s_{n-1}) \\ & \leq 2R(\mathcal{W}(\tilde{\varphi}_{n-2}^{-1} \circ \bar{\varphi}), \bar{m} - m_{n-2}, \bar{s} - s_{n-2}) + \bar{B}\mathcal{M}^4[R(\mathcal{W}(\tilde{\varphi}_{n-2}^{-1} \circ \bar{\varphi}), \bar{m} - m_{n-2}, \bar{s} - s_{n-2})] \\ 309 \quad & \leq B\mathcal{M}^4[R(\mathcal{W}(\tilde{\varphi}_{n-2}^{-1} \circ \bar{\varphi}), \bar{m} - m_{n-2}, \bar{s} - s_{n-2})] \\ & \leq \dots \\ & \leq B^{4n-3}\mathcal{M}^{4n}[R(\mathcal{W}(\tilde{\varphi}_0^{-1} \circ \bar{\varphi}), \bar{m} - m_0, \bar{s} - s_0)]. \end{aligned}$$

310 Define $M \triangleq \mathcal{M}[R(\mathcal{W}(\tilde{\varphi}_0^{-1} \circ \bar{\varphi}), \bar{m} - m_0, \bar{s} - s_0)]$. By (2.9) and (2.16), we then obtain $1 - C_1 \leq 0$
311 as $n \rightarrow +\infty$, which contradicts $C_1 \in (0, 1)$. Therefore, $\delta = \phi$. ■

312 *Remark 2.7.* By Theorem 2.6, the multiscale approach (2.1)-(2.2) provides a solution to
313 the following ‘greedy problem’:

$$314 \quad (2.17) \quad \inf_{(\mathbf{u}, m, s) \in \mathcal{L}(\Omega)} S_{lc}(\mathbf{u}, m, s).$$

315 Here, a key point is that the regularization in (2.17) is reflected on $\mathcal{L}(\Omega) = \mathcal{A}(\Omega) \times \mathcal{C}_\Omega \times SV_0(\Omega)$.
 316 Otherwise, the trivial solution (i.e., $\mathbf{u} = \mathbf{0}$, $m = \frac{T}{D}$, $s = 0$) may occur. In our method, some
 317 constraints (i.e., $\mathbf{u} \in \mathcal{A}(\Omega)$, $m \in \mathcal{C}_\Omega$, $s \in SV_0(\Omega)$) are additionally added in (1.4)-(1.6).
 318 Compared with the greedy problem in [21] that has nothing to do with parameters, the result
 319 of the greedy problem (2.17) is affected by two parameters K_1 and K_2 , since the constraint
 320 \mathcal{C}_Ω is determined by parameters K_1 and K_2 . In applications, a practitioner needs to give some
 321 estimates on the intensity of varying illumination and set suitable K_1, K_2 (i.e., K_1, K_2 are
 322 suggested to be set near zero if no varying illumination in image pairs), then the multiscale
 323 approach (2.1)-(2.2) can work well to produce some expected solutions.

324 **3. Alternating direction method for (2.2).** In this section, we mainly focus on the numer-
 325 ical implementation of the proposed multiscale approach (2.1)-(2.2) with λ_n and ε_n chosen
 326 by Theorem 2.6 (i.e., $\lambda_n = a^n \times b^{4^n}$ for some $a, b > 1$ and $\varepsilon_n = \frac{\varepsilon_0}{2^n}$ for some $\varepsilon_0 \in (0, 1)$). To
 327 address the non-convexity of $S_{lc}(\mathbf{u}, m, s)$, an auxiliary variable \mathbf{v} is additionally introduced
 328 and (2.2) is reformulated as follows

$$329 \quad (3.1) \quad (\mathbf{v}_n, \mathbf{u}_n, \delta m_n, \delta s_n) \in \underset{(\mathbf{v}, \mathbf{u}, m_{n-1} + m, s_{n-1} + s) \in \bar{\mathcal{L}}_{\varepsilon_n}(\Omega)}{\arg \min} E_n(\mathbf{v}, \mathbf{u}, m, s),$$

330 where

$$331 \quad E_n(\mathbf{v}, \mathbf{u}, m, s) = \lambda_n \int_{\Omega} (m_{n-1}(\mathbf{x}) + m(\mathbf{x}) + \ln D(\mathbf{x}) - \ln(T \circ \tilde{\varphi}_{n-1}(\mathbf{x} + \mathbf{v}(\mathbf{x})) - s_{n-1}(\mathbf{x}) - s(\mathbf{x})))^2 d\mathbf{x} \\
 332 \quad \quad \quad + \mu R(\mathbf{u}, m, s) + \Theta R_c(\mathbf{u}) + \frac{1}{2\theta_n} \int_{\Omega} |\mathbf{v} - \mathbf{u}|^2 d\mathbf{x},$$

334 $R_c(\mathbf{u}) = \int_{\Omega} \left(\frac{\partial u_1}{\partial x_1} - \frac{\partial u_2}{\partial x_2} \right)^2 + \left(\frac{\partial u_1}{\partial x_2} + \frac{\partial u_2}{\partial x_1} \right)^2 d\mathbf{x}$, $\bar{\mathcal{L}}_{\varepsilon_n}(\Omega) = L^2(\Omega) \times \mathcal{L}_{\varepsilon_n}(\Omega)$, $\theta_n > 0$ is a small
 335 number, and $\Theta > 0$ is a large number.

336 *Remark 3.1.* Here the penalty term $R_c(\mathbf{u})$ comes from [19] to relax the conformal con-
 337 straint. In fact, $R_c(\mathbf{u}) = 0$ when $\varphi(\mathbf{x}) = \mathbf{x} + \mathbf{u}(\mathbf{x})$ is in conformal set. Therefore, $R_c(\mathbf{u}) =$
 338 $\int_{\Omega} \left(\frac{\partial u_1}{\partial x_1} - \frac{\partial u_2}{\partial x_2} \right)^2 + \left(\frac{\partial u_1}{\partial x_2} + \frac{\partial u_2}{\partial x_1} \right)^2 d\mathbf{x}$ can be viewed as the distance between the mapping φ
 339 and conformal set. In this view, by setting some approximate regularization, the relaxed
 340 model (2.1) in [19] is equivalent to the quasi-conformal model in [40] which also minimizes the
 341 distance

$$342 \quad (3.2) \quad \int_{\Omega} \frac{\|\nabla \varphi(\mathbf{x})\|_F^2}{2 \det(\nabla \varphi(\mathbf{x}))} d\mathbf{x}$$

344 between mapping φ and conformal set in some sense. To illustrate this idea, the comparison
 345 results for these two models are listed on Fig 3. In this comparison, one can note that the
 346 relaxed model [19] and the quasi-conformal model [40] achieve the same type of deformation.
 347 Besides, the distance defined in (3.2) has the ability to control the minimal value of $\det(\nabla \varphi)$
 348 (because $\det(\nabla \varphi)$ acts as the denominator of the objective functional) while the distance
 349 $R_c(\mathbf{u})$ does not work on this aspect. That is, $R_c(\mathbf{u})$ controls less than (3.2). This is the reason
 350 why the relaxed model [19] achieves a lower quality (smaller $\min_{\mathbf{x} \in \Omega} \det(\nabla \varphi(\mathbf{x}))$) deformation,

351 but smaller Re – SSD. Moreover, the relaxed model also works for the landmark registration
 352 by deleting the fidelity term of the relaxed model [19] (Fig 4). Based on these comparisons
 353 and to make further analysis much easier, we use the relaxed conformal constraint $R_c(\mathbf{u})$ (with
 354 much simple structure) to control the mesh folding in this paper.

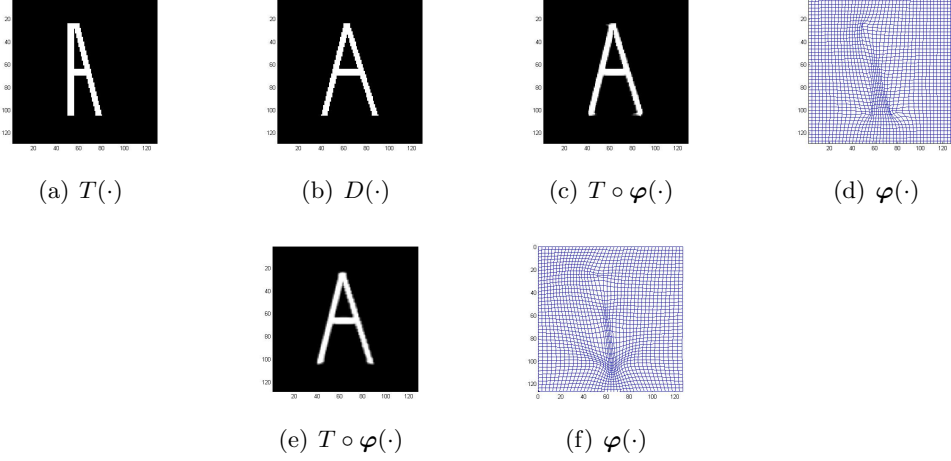


Figure 3. Comparison between the relaxed Cauchy-Riemann model [19] and the Quasi-conformal model [40]: (a)-(b) are floating image and target image, respectively; (c)-(d) are registration results of the relaxed Cauchy-Riemann model [19] with Re-SSD = 3.21%; (e)-(f) are registration results of the Quasi-conformal model [40] with Re-SSD = 4.63%.

355 Then setting an initialization $\mathbf{v}_n^0 = \mathbf{0}$, $\mathbf{u}_n^0 = \mathbf{0}$, $\delta m_n^0 = 0$, $\delta s_n^0 = 0$ for some given scale n ,
 356 (3.1) can be split into the following four subproblems

$$357 \quad (3.3) \quad \mathbf{v}_n^{k+1} \in \arg \min_{\mathbf{v} \in [L^2(\Omega)]^2} E_n(\mathbf{v}, \mathbf{u}_n^k, \delta m_n^k, \delta s_n^k),$$

$$358 \quad (3.4) \quad \mathbf{u}_n^{k+1} \in \arg \min_{\mathbf{u} \in [H_0^\alpha(\Omega)]^2} E_n(\mathbf{v}_n^{k+1}, \mathbf{u}, \delta m_n^k, \delta s_n^k),$$

$$359 \quad (3.5) \quad \delta m_n^{k+1} = \arg \min_{m_{n-1} + m \in \mathcal{C}_\Omega} E_n(\mathbf{v}_n^{k+1}, \mathbf{u}_n^{k+1}, m, \delta s_n^k),$$

$$360 \quad (3.6) \quad \delta s_n^{k+1} = \arg \min_{s_{n-1} + s \in SV_0(\Omega)} E_n(\mathbf{v}_n^{k+1}, \mathbf{u}_n^{k+1}, \delta m_n^{k+1}, s),$$

361
 362 for $k = 0, 1, 2, \dots$.

363 Concerning the convergence of $\{(\mathbf{v}_n^k, \mathbf{u}_n^k, \delta m_n^k, \delta s_n^k)\}$, here, we assume $\alpha > 3$ for the techni-
 364 cal demand to ensure $\varphi \in [C^2(\Omega)]^2$ ($H_0^\alpha(\Omega) \hookrightarrow C^2(\Omega)$ ($\alpha > 3$), Theorem 4.58 in [10]). Before
 365 showing the convergence result, we give some lemmas for subproblems (3.3)-(3.6), which will
 366 be used in the later proof.

367 **Lemma 3.2.** Suppose $\alpha > 3$, $T(\cdot)$ is twice differentiable with $\text{ess sup}_{\mathbf{x} \in \Omega} |T(\mathbf{x})| < \bar{M} < +\infty$,
 368 $\text{ess sup}_{\mathbf{x} \in \Omega} |D(\mathbf{x})| < \bar{M} < +\infty$, $0 < \theta_n < \frac{(\kappa - \kappa_0)^2}{10\bar{M}^2(\lambda_n \bar{M})^n}$, $\text{ess sup}_{\mathbf{x} \in \Omega} |\nabla T(\mathbf{x})| < \bar{M} < +\infty$ and
 369 $\text{ess sup}_{\mathbf{x} \in \Omega} |\nabla^2 T(\mathbf{x})| < \bar{M} < +\infty$, where $\bar{M} \triangleq \widetilde{M}(\Omega, \alpha) = 2C|\Omega|[K^2 + \ln^2(\bar{M}/\kappa)^2] > 0$, $K =$

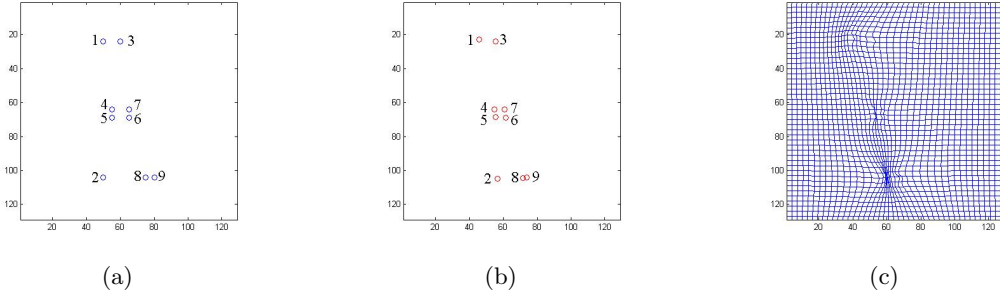


Figure 4. Landmark registration by the relaxed Cauchy-Riemann model [19]: (a)-(b) are the labels for the floating image and target image ($\varphi(\mathbf{x}_i) = \mathbf{y}_i (i = 1, 2, \dots, 9)$), respectively; (c) is the deformation induced by deleting the fidelity term of the relaxed Cauchy-Riemann model [19].

370 $\max\{|K_1|, |K_2|\}$ and $C = C(\Omega, \alpha)$ is a positive constant (see Lemma 3.2 and 3.3 in [17] for
 371 details). Then for the subproblem (3.3), there exists a constant $c > 0$ such that

$$372 \quad (3.7) \quad -2\lambda_n(m_{n-1} + m_n^k + \ln D - \ln T_n^{k+1}) \frac{\nabla_{\mathbf{v}} T \circ \tilde{\varphi}_{n-1}(\mathbf{x} + \mathbf{v}_n^{k+1})}{T_n^{k+1}} + \frac{1}{\theta_n}(\mathbf{v}_n^{k+1} - \mathbf{u}_n^k) = 0$$

373 and

$$374 \quad E_n(\mathbf{v}_n^k, \mathbf{u}_n^k, \delta m_n^k, \delta s_n^k) - E_n(\mathbf{v}_n^{k+1}, \mathbf{u}_n^k, \delta m_n^k, \delta s_n^k) \geq c \|\mathbf{v}_n^{k+1} - \mathbf{v}_n^k\|_{[L^2(\Omega)]^2}^2.$$

375 Here and in what follows, $T_n^{k+1} = T \circ \tilde{\varphi}_{n-1}(\mathbf{x} + \mathbf{v}_n^{k+1}) - s_{n-1} - \delta s_n^k$.

376 *Proof.* The first-order variation of (3.3) is

$$377 \quad (3.8) \quad -2\lambda_n \int_{\Omega} (m_{n-1} + m_n^k + \ln D - \ln T_n^{k+1}) \frac{\nabla_{\mathbf{v}} T \circ \tilde{\varphi}_{n-1}(\mathbf{x} + \mathbf{v}_n^{k+1})}{T_n^{k+1}} \cdot \mathbf{z}(\mathbf{x}) d\mathbf{x} \\ + \frac{1}{\theta_n} \int_{\Omega} (\mathbf{v}_n^{k+1} - \mathbf{u}_n^k) \cdot \mathbf{z}(\mathbf{x}) d\mathbf{x} = 0,$$

378 where \mathbf{z} is the test function. By the variational principle, this concludes (3.7).

379 Letting $\mathbf{z} = \mathbf{v}_n^k - \mathbf{v}_n^{k+1}$ in (3.8), it yields

$$380 \quad L(\mathbf{v}_n^k, \mathbf{v}_n^{k+1}) = \int_{\Omega} (-2\lambda_n(m_{n-1} + \delta m_n^k + \ln D - \ln T_n^{k+1}) \frac{\nabla_{\mathbf{v}} T \circ \tilde{\varphi}_{n-1}(\mathbf{x} + \mathbf{v}_n^{k+1})}{T_n^{k+1}} \\ + \frac{1}{\theta_n}(\mathbf{v}_n^{k+1} - \mathbf{u}_n^k)) \cdot (\mathbf{v}_n^k - \mathbf{v}_n^{k+1}) d\mathbf{x} = 0.$$

381 Then we have

$$382 \quad (3.9) \quad E_n(\mathbf{v}_n^k, \mathbf{u}_n^k, \delta m_n^k, \delta s_n^k) - E_n(\mathbf{v}_n^{k+1}, \mathbf{u}_n^k, \delta m_n^k, \delta s_n^k) \\ = \lambda_n \int_{\Omega} \ln \frac{T \circ \tilde{\varphi}_{n-1}(\mathbf{x} + \mathbf{v}_n^{k+1}) - s_{n-1} - \delta s_n^k}{T \circ \tilde{\varphi}_{n-1}(\mathbf{x} + \mathbf{v}_n^k) - s_{n-1} - \delta s_n^k} \cdot (2m_{n-1} + 2\delta m_n^k + 2 \ln D - 2 \ln T_n^{k+1} \\ + \ln \frac{T \circ \tilde{\varphi}_{n-1}(\mathbf{x} + \mathbf{v}_n^{k+1}) - s_{n-1} - \delta s_n^k}{T \circ \tilde{\varphi}_{n-1}(\mathbf{x} + \mathbf{v}_n^k) - s_{n-1} - \delta s_n^k}) d\mathbf{x} + \frac{1}{2\theta_n} \int_{\Omega} (\mathbf{v}_n^k - \mathbf{v}_n^{k+1}) \cdot (\mathbf{v}_n^k + \mathbf{v}_n^{k+1} - 2\mathbf{u}_n^k) d\mathbf{x}.$$

383 By using the Taylor's formula, we get

$$384 \quad (3.10) \quad \ln(T \circ \tilde{\varphi}_{n-1}(\mathbf{x} + \mathbf{v}_n^{k+1}) - s_{n-1} - \delta s_n^k) = \ln(T \circ \tilde{\varphi}_{n-1}(\mathbf{x} + \mathbf{v}_n^k) - s_{n-1} - \delta s_n^k) + A + B,$$

385 where $A = \frac{\nabla_{\mathbf{v}} T \circ \tilde{\varphi}_{n-1}(\mathbf{x} + \mathbf{v}_n^k) \cdot (\mathbf{v}_n^{k+1} - \mathbf{v}_n^k)}{T \circ \tilde{\varphi}_{n-1}(\mathbf{x} + \mathbf{v}_n^k) - s_{n-1} - \delta s_n^k}$, $B = (\mathbf{v}_n^k - \mathbf{v}_n^{k+1})H(\sigma)(\mathbf{v}_n^k - \mathbf{v}_n^{k+1})^T$, and $H(\sigma)$ is the
 386 Hessian matrix of the function $\ln(T \circ \tilde{\varphi}_{n-1}(\mathbf{x} + \mathbf{v}_n^k) - s_{n-1} - \delta s_n^k)$ on the point σ between
 387 \mathbf{v}_n^k and \mathbf{v}_n^{k+1} . Note that here we use the condition $\alpha > 3$ for technical demand to ensure
 388 $H_0^\alpha(\Omega) \hookrightarrow C^2(\Omega)$ (Theorem 4.58 in [10]). Due to $\varphi_n \in [H_0^\alpha(\Omega)]^2$, we have $\tilde{\varphi}_n \in [C^2(\Omega)]^2$,
 389 which implies $T \circ \varphi_n \in C^2(\Omega)$. This makes the Hessian matrix $H(\cdot)$ of $T \circ \varphi_n \in C^2(\Omega)$ well
 390 defined.

391 Hence, by (3.9) and (3.10), there holds

$$392 \quad \begin{aligned} & E_n(\mathbf{v}_n^k, \mathbf{u}_n^k, \delta m_n^k, \delta s_n^k) - E_n(\mathbf{v}_n^{k+1}, \mathbf{u}_n^k, \delta m_n^k, \delta s_n^k) \\ & \geq \lambda_n \int_{\Omega} (A + B)^2 d\mathbf{x} + c \|\mathbf{v}_n^{k+1} - \mathbf{v}_n^k\|_{[L^2(\Omega)]^2}^2 + L(\mathbf{v}_n^k, \mathbf{v}_n^{k+1}) \geq c \|\mathbf{v}_n^{k+1} - \mathbf{v}_n^k\|_{[L^2(\Omega)]^2}^2, \end{aligned}$$

393 where $c = \frac{1}{2\theta_n} - c_0 > 0$ and $c_0 = \|H(\sigma)\|_{L^\infty(\Omega)} = \frac{10\bar{M}^2(\lambda_n \bar{M})^n}{(\kappa - \kappa_0)^2}$ (see Appendix A for details). ■

394 **Lemma 3.3.** *For the subproblem (3.4), there holds*

$$(3.11) \quad \begin{aligned} & 2\mu \int_{\Omega} \nabla^\alpha \mathbf{u}_n^{k+1} \cdot \nabla^\alpha \mathbf{w} d\mathbf{x} + 2\Theta \int_{\Omega} \left(\frac{\partial u_{n,1}^{k+1}}{\partial x_1} - \frac{\partial u_{n,2}^{k+1}}{\partial x_2} \right) \cdot \left(\frac{\partial w_1^{k+1}}{\partial x_1} - \frac{\partial w_2^{k+1}}{\partial x_2} \right) d\mathbf{x} \\ 395 & + 2\Theta \int_{\Omega} \left(\frac{\partial u_{n,1}^{k+1}}{\partial x_2} + \frac{\partial u_{n,2}^{k+1}}{\partial x_1} \right) \cdot \left(\frac{\partial w_1^{k+1}}{\partial x_2} + \frac{\partial w_2^{k+1}}{\partial x_1} \right) d\mathbf{x} - \frac{1}{\theta_n} \int_{\Omega} (\mathbf{v}_n^{k+1} - \mathbf{u}_n^{k+1}) \cdot \mathbf{w} d\mathbf{x} = 0, \end{aligned}$$

396 for any $\mathbf{w} \in [C_0^\infty(\Omega)]^2$, and

$$397 \quad E_n(\mathbf{v}_n^{k+1}, \mathbf{u}_n^k, \delta m_n^k, \delta s_n^k) - E_n(\mathbf{v}_n^{k+1}, \mathbf{u}_n^{k+1}, \delta m_n^k, \delta s_n^k) \geq c_1 \|\mathbf{u}_n^k - \mathbf{u}_n^{k+1}\|_{[H_0^\alpha(\Omega)]^2}^2,$$

398 for some $c_1 > 0$.

399 *Proof.* The first-order variation of (3.4) is

$$400 \quad \begin{aligned} & 2\mu \int_{\Omega} \nabla^\alpha \mathbf{u}_n^{k+1} \cdot \nabla^\alpha \mathbf{w} d\mathbf{x} + 2\Theta \int_{\Omega} \left(\frac{\partial u_{n,1}^{k+1}}{\partial x_1} - \frac{\partial u_{n,2}^{k+1}}{\partial x_2} \right) \cdot \left(\frac{\partial w_1^{k+1}}{\partial x_1} - \frac{\partial w_2^{k+1}}{\partial x_2} \right) d\mathbf{x} \\ & + 2\Theta \int_{\Omega} \left(\frac{\partial u_{n,1}^{k+1}}{\partial x_2} + \frac{\partial u_{n,2}^{k+1}}{\partial x_1} \right) \cdot \left(\frac{\partial w_1^{k+1}}{\partial x_2} + \frac{\partial w_2^{k+1}}{\partial x_1} \right) d\mathbf{x} - \frac{1}{\theta_n} \int_{\Omega} (\mathbf{v}_n^{k+1} - \mathbf{u}_n^{k+1}) \cdot \mathbf{w} d\mathbf{x} = 0, \end{aligned}$$

401 where $\mathbf{w} = (w_1, w_2)^T$ is a test function. This concludes (3.11).

402 Letting $\mathbf{w} = \mathbf{u}_n^k - \mathbf{u}_n^{k+1}$, then there holds

(3.12)

$$\begin{aligned}
 \tilde{L}(\mathbf{u}_n^k, \mathbf{u}_n^{k+1}) &= 2\mu \int_{\Omega} \nabla^{\alpha} \mathbf{u}_n^{k+1} \cdot \nabla^{\alpha} (\mathbf{u}_n^k - \mathbf{u}_n^{k+1}) d\mathbf{x} + \frac{1}{\theta_n} \int_{\Omega} (\mathbf{u}_n^{k+1} - \mathbf{v}_n^{k+1}) \cdot (\mathbf{u}_n^k - \mathbf{u}_n^{k+1}) d\mathbf{x} \\
 &+ 2\Theta \int_{\Omega} \left(\frac{\partial u_{n,1}^{k+1}}{\partial x_1} - \frac{\partial u_{n,2}^{k+1}}{\partial x_2} \right) \left(\frac{\partial u_{n,1}^k}{\partial x_1} - \frac{\partial u_{n,2}^k}{\partial x_2} \right) d\mathbf{x} \\
 &+ 2\Theta \int_{\Omega} \left(\frac{\partial u_{n,1}^{k+1}}{\partial x_2} + \frac{\partial u_{n,2}^{k+1}}{\partial x_1} \right) \left(\frac{\partial u_{n,1}^k}{\partial x_2} + \frac{\partial u_{n,2}^k}{\partial x_1} \right) d\mathbf{x} \\
 &- 2\Theta \int_{\Omega} \left(\frac{\partial u_{n,1}^{k+1}}{\partial x_1} - \frac{\partial u_{n,2}^{k+1}}{\partial x_2} \right)^2 d\mathbf{x} - 2\Theta \int_{\Omega} \left(\frac{\partial u_{n,1}^{k+1}}{\partial x_2} + \frac{\partial u_{n,2}^{k+1}}{\partial x_1} \right)^2 d\mathbf{x} = 0.
 \end{aligned}$$

404 Therefore, based on (3.12), we obtain

$$\begin{aligned}
 &E_n(\mathbf{v}_n^{k+1}, \mathbf{u}_n^k, \delta m_n^k, \delta s_n^k) - E_n(\mathbf{v}_n^{k+1}, \mathbf{u}_n^{k+1}, \delta m_n^k, \delta s_n^k) \\
 (3.13) \quad &\geq \mu \|\nabla^{\alpha} (\mathbf{u}_n^k - \mathbf{u}_n^{k+1})\|_{[L^2(\Omega)]^2}^2 + \frac{1}{2\theta_n} \|\mathbf{u}_n^k - \mathbf{u}_n^{k+1}\|_{[L^2(\Omega)]^2}^2 + \tilde{L}(\mathbf{u}_n^k, \mathbf{u}_n^{k+1}) \\
 &\geq c_1 \|\mathbf{u}_n^k - \mathbf{u}_n^{k+1}\|_{[H_0^{\alpha}(\Omega)]^2}^2.
 \end{aligned}$$

409 **Lemma 3.4.** For subproblems (3.5) and (3.6), there holds

$$(3.14) \quad 2\lambda_n (m_{n-1} + \delta m_n^{k+1} + \ln D - \ln T_n^{k+1}) - \mu \operatorname{div} \left(\frac{\delta m_n^{k+1}}{|\delta m_n^{k+1}|} \right) = 0,$$

$$(3.15) \quad 2\lambda_n (m_{n-1} + \delta m_n^{k+1} + \ln D - \ln \tilde{T}_n^{k+1}) \frac{1}{\tilde{T}_n^{k+1}} - \mu \operatorname{div} \left(\frac{\nabla \delta s_n^{k+1}}{|\nabla \delta s_n^{k+1}|} \right) = 0,$$

$$(3.16) \quad E_n(\mathbf{v}_n^{k+1}, \mathbf{u}_n^{k+1}, \delta m_n^k, \delta s_n^k) - E_n(\mathbf{v}_n^{k+1}, \mathbf{u}_n^{k+1}, \delta m_n^{k+1}, \delta s_n^k) \geq \lambda_n \|\delta m_n^k - \delta m_n^{k+1}\|_{L^2(\Omega)}^2,$$

414 and

$$(3.17) \quad E_n(\mathbf{v}_n^{k+1}, \mathbf{u}_n^{k+1}, \delta m_n^{k+1}, \delta s_n^k) - E_n(\mathbf{v}_n^{k+1}, \mathbf{u}_n^{k+1}, \delta m_n^{k+1}, \delta s_n^{k+1}) \geq \lambda_n \|\delta s_n^k - \delta s_n^{k+1}\|_{L^2(\Omega)}^2,$$

417 where $\tilde{T}_n^{k+1} = T \circ \tilde{\varphi}_{n-1}(\mathbf{x} + \mathbf{v}_n^{k+1}) - s_{n-1} - \delta s_n^{k+1}$.

418 *Proof.* The first-order variation of (3.5) is

$$2\lambda_n \int_{\Omega} (m_{n-1} + \delta m_n^{k+1} + \ln D - \ln T_n^{k+1}) \cdot p d\mathbf{x} + \mu \int_{\Omega} \frac{\nabla \delta m_n^{k+1} \cdot \nabla p}{|\nabla \delta m_n^{k+1}|} d\mathbf{x} = 0,$$

420 where p is the test function. By using the integration-by-parts formula [14], we get (3.14).

421 Letting $p = \delta m_n^k - \delta m_n^{k+1}$, we have

$$\begin{aligned}
 \hat{L} &= 2\lambda_n \int_{\Omega} [m_{n-1} + \delta m_n^{k+1} + \ln D - \ln T_n^{k+1}] \cdot (\delta m_n^k - \delta m_n^{k+1}) d\mathbf{x} \\
 &+ \mu \int_{\Omega} \frac{\nabla \delta m_n^{k+1} \cdot \nabla (\delta m_n^k - \delta m_n^{k+1})}{|\nabla \delta m_n^{k+1}|} d\mathbf{x} = 0.
 \end{aligned}$$

423 Then we obtain

$$424 \quad \begin{aligned} & E_n(\mathbf{v}_n^{k+1}, \mathbf{u}_n^{k+1}, \delta m_n^k, \delta s_n^k) - E_n(\mathbf{v}_n^{k+1}, \mathbf{u}_n^{k+1}, \delta m_n^{k+1}, \delta s_n^k) \\ & \geq \lambda_n \|\delta m_n^k - \delta m_n^{k+1}\|_{L^2(\Omega)}^2 + \hat{L} = \lambda_n \|\delta m_n^k - \delta m_n^{k+1}\|_{L^2(\Omega)}^2. \end{aligned}$$

425 Further, by giving similar analysis on the subproblem (3.6), we conclude (3.15) and (3.17). ■

426 Now, based on Lemmas 3.2-3.4, we give the convergence result of the sequence $\{(\mathbf{v}_n^k, \mathbf{u}_n^k,$
427 $\delta m_n^k, \delta s_n^k)\}$.

428 **Theorem 3.5.** Assume that the conditions in Lemmas 3.2-3.4 are satisfied, then the se-
429 quence $\{(\mathbf{v}_n^k, \mathbf{u}_n^k, \delta m_n^k, \delta s_n^k)\}$ generated by (3.3)-(3.6) converges to the solution of (3.1) when
430 $k \rightarrow +\infty$.

431 *Proof.* First, we claim that there exists $(\mathbf{v}_n, \mathbf{u}_n, \delta m_n, \delta s_n) \in [L^2(\Omega)]^2 \times [H_0^\alpha(\Omega)]^2 \times \mathcal{C}_\Omega \times$
432 $SV_0(\Omega)$ such that

$$433 \quad (3.18) \quad \begin{aligned} & \mathbf{v}_n^k \xrightarrow{k} \mathbf{v}_n \text{ in } [L^2(\Omega)]^2, \quad \mathbf{u}_n^k \xrightarrow{k} \mathbf{u}_n \text{ in } [H_0^\alpha(\Omega)]^2, \\ & \delta m_n^k \xrightarrow{k} \delta m_n \text{ in } \mathcal{C}_\Omega, \quad \delta s_n^k \xrightarrow{k} \delta s_n \text{ in } SV_0(\Omega). \end{aligned}$$

434 By Lemmas 3.2-3.4, we obtain that

$$435 \quad (3.19) \quad \begin{aligned} & E_n(\mathbf{v}_n^k, \mathbf{u}_n^k, \delta m_n^k, \delta s_n^k) - E_n(\mathbf{v}_n^{k+1}, \mathbf{u}_n^{k+1}, \delta m_n^{k+1}, \delta s_n^{k+1}) \\ & \geq c \|\mathbf{v}_n^k - \mathbf{v}_n^{k+1}\|_{[L^2(\Omega)]^2}^2 + c_1 \|\mathbf{u}_n^k - \mathbf{u}_n^{k+1}\|_{[H_0^\alpha(\Omega)]^2}^2 \\ & \quad + \lambda_n \|\delta m_n^k - \delta m_n^{k+1}\|_{L^2(\Omega)}^2 + \lambda_n \|\delta s_n^k - \delta s_n^{k+1}\|_{L^2(\Omega)}^2. \end{aligned}$$

436 Note that $E_n(\mathbf{v}_n^k, \mathbf{u}_n^k, \delta m_n^k, \delta s_n^k)$ is a decreasing sequence with a lower bound, which implies
437 that the left side of (3.19) converges to zero when $k \rightarrow +\infty$. Hence, we have,

$$438 \quad (3.20) \quad \begin{aligned} & \|\mathbf{v}_n^k - \mathbf{v}_n^{k+1}\|_{[L^2(\Omega)]^2}^2 \xrightarrow{k} 0, \quad \|\mathbf{u}_n^k - \mathbf{u}_n^{k+1}\|_{[H_0^\alpha(\Omega)]^2}^2 \xrightarrow{k} 0, \\ & \|\delta m_n^k - \delta m_n^{k+1}\|_{L^2(\Omega)}^2 \xrightarrow{k} 0, \quad \|\delta s_n^k - \delta s_n^{k+1}\|_{L^2(\Omega)}^2 \xrightarrow{k} 0, \end{aligned}$$

439 as $k \rightarrow +\infty$. Then by the compactness of Banach space $L^2(\Omega)$, $H_0^\alpha(\Omega)$, there exists $(\mathbf{v}_n, \mathbf{u}_n,$
440 $\delta m_n, \delta s_n) \in [L^2(\Omega)]^2 \times [H_0^\alpha(\Omega)]^2 \times L^2(\Omega) \times L^2(\Omega)$ such that

$$441 \quad \begin{aligned} & \mathbf{v}_n^k \xrightarrow{k} \mathbf{v}_n \text{ in } [L^2(\Omega)]^2, \quad \mathbf{u}_n^k \xrightarrow{k} \mathbf{u}_n \text{ in } [H_0^\alpha(\Omega)]^2, \\ & \delta m_n^k \xrightarrow{k} \delta m_n \text{ in } L^2(\Omega), \quad \delta s_n^k \xrightarrow{k} \delta s_n \text{ in } L^2(\Omega). \end{aligned}$$

442 In addition, since δm_n^k is bounded in $BV(\Omega)$, there exists a subsequence of δm_n^k which are
443 still labelled with δm_n^k and $\delta \bar{m}_n \in BV_0(\Omega)$ such that

$$444 \quad (3.21) \quad \|\delta m_n^k - \delta \bar{m}_n\|_{L^1(\Omega)} \xrightarrow{k} 0, \quad \int_\Omega \nabla \delta m_n^k \cdot w \, d\mathbf{x} \xrightarrow{k} \int_\Omega \nabla \delta \bar{m}_n \cdot w \, d\mathbf{x},$$

445 for any $w \in C_0^\infty(\Omega)$. By (3.20), (3.21) and the uniqueness of the limit for m_n^k , there holds
446 $\delta m_n = \delta \bar{m}_n \in BV_0(\Omega)$. So we have $m_{n-1} + \delta m_n \in \mathcal{C}_\Omega$. Similarly, we also have $s_{n-1} + \delta s_n \in$
447 $SV_0(\Omega)$. Therefore, we obtain the claim (3.18).

448 Next, we claim that $(\mathbf{v}_n, \mathbf{u}_n, \delta m_n, \delta s_n)$ is a minimizer of (3.1).

449 By (3.7), (3.11) and (3.18), we know that

$$450 \quad (3.22) \quad -2\lambda_n[m_{n-1} + m_n + \ln D - \ln T_n] \frac{\nabla_{\mathbf{v}} T \circ \tilde{\varphi}_{n-1}(\mathbf{x} + \mathbf{v}_n)}{T_n} + \frac{1}{\theta_n}(\mathbf{v}_n - \mathbf{u}_n) = 0$$

451 and

$$452 \quad (3.23) \quad \begin{aligned} & 2\mu \int_{\Omega} \nabla^{\alpha} \mathbf{u}_n \cdot \nabla^{\alpha} \mathbf{z} d\mathbf{x} + 2\Theta \int_{\Omega} \left(\frac{\partial u_{n,1}}{\partial x_1} - \frac{\partial u_{n,2}}{\partial x_2} \right) \cdot \left(\frac{\partial z_1}{\partial x_1} - \frac{\partial z_2}{\partial x_2} \right) d\mathbf{x} \\ & + 2\Theta \int_{\Omega} \left(\frac{\partial u_{n,1}}{\partial x_2} + \frac{\partial u_{n,2}}{\partial x_1} \right) \cdot \left(\frac{\partial z_1}{\partial x_2} + \frac{\partial z_2}{\partial x_1} \right) d\mathbf{x} - \frac{1}{\theta_n} \int_{\Omega} (\mathbf{v}_n - \mathbf{u}_n) \cdot \mathbf{z} d\mathbf{x} = 0, \end{aligned}$$

453 where $T_n = T \circ \tilde{\varphi}_{n-1}(\mathbf{x} + \mathbf{v}_n) - s_{n-1} - \delta s_n$. By (3.14), we also obtain

$$454 \quad 2\lambda_n[m_{n-1} + \delta m_n^{k+1} + \ln D - \ln T_n^{k+1}] + \mathcal{H}(\delta m_n^{k+1}) = 0,$$

455 where $\mathcal{H}(m_n^{k+1}) = -\mu \operatorname{div} \left(\frac{\nabla \delta m_n^{k+1}}{|\nabla \delta m_n^{k+1}|} \right)$. This implies

$$456 \quad \mathcal{H}(\delta m_n^{k+1}) \xrightarrow{k} -2\lambda_n[m_{n-1} + \delta m_n + \ln D - \ln T_n] \triangleq \mathcal{T}.$$

457 Note that \mathcal{H} is a monotone operator because \mathcal{H} is the derivative of a convex functional, which
458 shows

$$459 \quad \int_{\Omega} [\mathcal{H}(\delta m_n^{k+1}) - \mathcal{H}(\omega)] \cdot (\delta m_n^{k+1} - \omega) d\mathbf{x} \geq 0, \quad \forall \omega \in BV(\Omega).$$

460 Furthermore, there holds

$$461 \quad \int_{\Omega} \mathcal{H}(\delta m_n^{k+1}) \cdot \delta m_n^{k+1} d\mathbf{x} \xrightarrow{k} \int_{\Omega} \mathcal{T} \cdot \delta m_n d\mathbf{x},$$

462 and

$$463 \quad \int_{\Omega} \mathcal{H}(\omega) \cdot \delta m_n^{k+1} d\mathbf{x} \xrightarrow{k} \int_{\Omega} \mathcal{H}(\omega) \cdot \delta m_n d\mathbf{x}.$$

464 So we get

$$465 \quad \int_{\Omega} [\mathcal{T} - \mathcal{H}(\omega)] \cdot (\delta m_n - \omega) d\mathbf{x} \geq 0.$$

466 Let $\omega = \delta m_n + h\psi$ for any $\psi \in C_0^{\infty}(\Omega)$ and we have

$$467 \quad \int_{\Omega} [\mathcal{T} - \mathcal{H}(\delta m_n + h\psi)] \cdot \psi d\mathbf{x} \leq 0.$$

468 Besides,

$$469 \quad \int_{\Omega} \mathcal{H}(\delta m_n + h\psi) \cdot \psi d\mathbf{x} \xrightarrow{k} \int_{\Omega} \mathcal{H}(\delta m_n) \cdot \psi d\mathbf{x}$$

470 as $h \rightarrow 0$. Therefore,

$$471 \quad \int_{\Omega} \mathcal{T} \cdot \psi d\mathbf{x} \leq \int_{\Omega} \mathcal{H}(\delta m_n) \cdot \psi d\mathbf{x}.$$

472 So we have $\mathcal{H}(\delta m_n) = \mathcal{T}$ and

$$473 \quad (3.24) \quad 2\lambda_n[m_{n-1} + \delta m_n + \ln D - \ln T_n] + \mathcal{H}(\delta m_n) = 0.$$

474 In a similar way, there holds

$$475 \quad (3.25) \quad 2\lambda_n[m_{n-1} + \delta m_n + \ln D - \ln T_n] \frac{1}{T_n} - \mu \operatorname{div} \left(\frac{\nabla \delta s_n}{|\nabla \delta s_n|} \right) = 0.$$

476 Then by (3.22), (3.23), (3.24) and (3.25), we conclude that $(\mathbf{v}_n, \mathbf{u}_n, \delta m_n, \delta s_n)$ is a minimizer
477 of (3.1). ■

478 At the end of this section, we focus on the numerical implementation of the subproblem
479 (3.3)-(3.6). For some given domain $\Omega = (0, a) \times (0, a)$ and scale number n , we define $h = \frac{a}{N_S}$
480 for some given $N_S \in \mathbb{N}^+$. Here, we also define $(x_1)_i = ih$, $(x_2)_j = jh$ for $i, j = 0, 1, 2, \dots, N_S$
481 and $\mathbf{P}_{i,j} = ((x_1)_i, (x_2)_j)$ for $i, j = 0, 1, 2, \dots, N_S$.

482 **v-problem:** Define $r(\mathbf{v}) = m_{n-1} + \delta m_n^k + \ln D - \ln(T \circ \tilde{\varphi}_{n-1}(\mathbf{x} + \mathbf{v}(\mathbf{x})) - s_{n-1} - \delta s_n^k)$.
483 By using the Taylor's formula, there holds

$$484 \quad (3.26) \quad r(\mathbf{v}_n^{k+1}) \approx r(\mathbf{u}_n^k) - \mathbf{L}^k \cdot (\mathbf{v}_n^{k+1} - \mathbf{u}_n^k),$$

485 where $\mathbf{L}^k = (L_x, L_y)^T = \frac{1}{T \circ \tilde{\varphi}_{n-1}(\mathbf{x} + \mathbf{u}_n^k(\mathbf{x})) - s_{n-1} - \delta s_n^k} \nabla_{\mathbf{u}} T \circ \tilde{\varphi}_{n-1}(\mathbf{x} + \mathbf{u}_n^k(\mathbf{x}))$. Substituting (3.26)
486 into (3.3), we obtain the following Euler-Lagrange equation for (3.3)

$$487 \quad (3.27) \quad \mathbf{G} \mathbf{v}_n^{k+1} = \phi(\mathbf{u}_n^k), \quad \forall \mathbf{x} \in \Omega,$$

488 where

$$489 \quad \mathbf{G} = \begin{pmatrix} 1 + 2\lambda_{n-1}\theta_n L_x^2 & 2\lambda_{n-1}\theta_n L_x L_y \\ 2\lambda_{n-1}\theta_n L_x L_y & 1 + 2\lambda_{n-1}\theta_n L_y^2 \end{pmatrix}, \quad \mathbf{v}_n^{k+1} = \begin{pmatrix} v_{n,1}^{k+1} \\ v_{n,2}^{k+1} \end{pmatrix},$$

490

$$491 \quad \phi(\mathbf{u}_n^k) = \begin{pmatrix} u_{n,1}^k + 2\lambda_{n-1}\theta_n [r(\mathbf{u}_n^k)L_x + L_x^2 u_{n,1}^k + L_x L_y u_{n,2}^k] \\ u_{n,2}^k + 2\lambda_{n-1}\theta_n [r(\mathbf{u}_n^k)L_y + L_x L_y u_{n,1}^k + L_y^2 u_{n,2}^k] \end{pmatrix},$$

492 and $\mathbf{u}_n^k \triangleq (u_{n,1}^k, u_{n,2}^k)^T$. By solving the linear system (3.27), one gets the updated \mathbf{v}_n^{k+1} for
493 each $\mathbf{x} \in \Omega$.

494 **u-problem:** Based on the updated \mathbf{v}_n^{k+1} , the Euler-Lagrange equation for \mathbf{u} from (3.4) is
495 formulated as follows

$$496 \quad (3.28) \quad 2\mu\theta_n \operatorname{div}^{\alpha*}(\nabla^{\alpha} \mathbf{u}_n^{k+1}) - 2\Theta\theta_n \Delta \mathbf{u}_n^{k+1} + \mathbf{u}_n^{k+1} = \mathbf{v}_n^{k+1}, \quad \forall \mathbf{x} \in \Omega.$$

497 Concerning the numerical computation of (3.28), the multigrid method is used to accelerate
498 the algorithm. The details of the multigrid method for (3.28) are listed in Algorithm B.1 in
499 Appendix B.

500 **m -problem:** By ignoring the constant term, (3.5) is essentially equivalent to the following
 501 convex optimization problem

$$502 \quad (3.29) \quad \delta m_n^{k+1} = \arg \min_{m_{n-1}+m \in \mathcal{C}_\Omega} \frac{1}{2} \int_\Omega |g - m|^2 d\mathbf{x} + \frac{\mu}{2\lambda_{n-1}} \int_\Omega |\nabla m| d\mathbf{x}, \quad \forall \mathbf{x} \in \Omega,$$

504 where $g(\mathbf{x}) = \ln(T \circ \tilde{\varphi}_{n-1}(\mathbf{x} + \mathbf{v}^{k+1}) - s_{n-1}(\mathbf{x}) - \delta s_n^k(\mathbf{x})) - m_{n-1}(\mathbf{x}) - \ln D(\mathbf{x})$. Without the
 505 constraint $K_1 \leq m \leq K_2$, (3.29) is essentially a standard form of the total variation (TV)
 506 minimization. The solution of (3.29) (without constraint $K_1 \leq m \leq K_2$) is

$$507 \quad (3.30) \quad m = g - \mathcal{P}_{\lambda K}(g).$$

508 Note that here and in what follows, $\mathcal{P}_A(v)$ denotes the element in A which minimizes the
 509 distance between v and all the elements in A . Here we use the Chambolle Projection algorithm
 510 [2] to compute $\mathcal{P}_{\lambda K}(g)$. By giving the initial value $\mathbf{p}^0 = (0, 0)$, $0 < \tau < \frac{1}{8}$ and the following
 511 iterative sequence

$$512 \quad \mathbf{p}_{i,j}^{l+1} = \frac{\mathbf{p}_{i,j}^l + \tau \nabla(\operatorname{div} \mathbf{p}^l - g/\lambda)_{i,j}}{1 + \tau |\nabla(\operatorname{div} \mathbf{p}^l - g/\lambda)_{i,j}|},$$

513 we have $\lambda \operatorname{div} \mathbf{p}^l \rightarrow \mathcal{P}_{\lambda K}(g)$ with $l \rightarrow +\infty$ [2]. Then, based on (3.30), we get the solution of
 514 (3.29) by projecting the solution of (3.30) onto the set \mathcal{C}_Ω :

$$515 \quad (3.31) \quad (\delta m_n^{k+1})_{i,j} = \begin{cases} [g - \mathcal{P}_{\lambda K}(g)]_{i,j}, & K_1 \leq [g - \mathcal{P}_{\lambda K}(g)]_{i,j} \leq K_2, \\ K_1, & [g - \mathcal{P}_{\lambda K}(g)]_{i,j} < K_1, \\ K_2, & [g - \mathcal{P}_{\lambda K}(g)]_{i,j} > K_2, \end{cases}$$

516 for $i, j = 0, 1, 2, \dots, N_S$.

517 **s -problem:** Define $\mathcal{G}(\Omega) = \{s \in BV_0(\Omega) | s(\mathbf{x}) \leq \kappa - \kappa_0 - s_{n-1}(\mathbf{x}) \text{ for } \forall \mathbf{x} \in \Omega\}$. Then $\mathcal{G}(\Omega)$
 518 is a closed and convex set. Assume that δs_n is a solution of (3.4). Then for any $r \in \mathcal{G}(\Omega)$,
 519 there holds $\delta s_n + \tau(r - \delta s_n) = (1 - \tau)\delta s_n + \tau r \in \mathcal{G}(\Omega)$ for $0 \leq \tau \leq 1$. Next, we define
 520 $J(\tau) = E_n(\mathbf{v}_n^{k+1}, \mathbf{u}_n^{k+1}, \delta m_n^{k+1}, \delta s_n + \tau(r - \delta s_n))$, which yields

$$521 \quad J(0) \leq J(\tau), \quad \forall \tau \in [0, 1].$$

522 Therefore,

$$523 \quad (3.32) \quad 0 \leq J'(0) = \int_\Omega \mathcal{F}(\delta s_n) \cdot (r - \delta s_n) d\mathbf{x}, \quad \text{for } \forall r \in \mathcal{G},$$

524 where $\mathcal{F}(\delta s_n) = \frac{2\lambda_n(m_{n-1} + \delta m_n^{k+1} + \ln D - \ln(T \circ \tilde{\varphi}_{n-1}(\mathbf{x} + \mathbf{v}_n^{k+1}) - s_{n-1} - \delta s_n))}{T \circ \tilde{\varphi}_{n-1}(\mathbf{x} + \mathbf{v}_n^{k+1}) - s_{n-1} - \delta s_n} - \mu \operatorname{div} \left(\frac{\nabla \delta s_n}{|\nabla \delta s_n|} \right)$. Note that
 525 \mathcal{F} is a monotone operator [23] and (3.32) is equivalent to $\delta s_n = \mathcal{P}_{\mathcal{G}}[\delta s_n - \rho \mathcal{F}(\delta s_n)]$, which
 526 induces the following iterative method for (3.4):

$$527 \quad (3.33) \quad \delta s_n^{l+1} = \mathcal{P}_{\mathcal{G}}[\delta s_n^l - \rho \mathcal{F}(\delta s_n^l)], \quad l = 0, 1, 2, \dots,$$

529 with $\varrho > 0$. Concerning the projection in (3.33), it is essential to solve the following optimiza-
530 tion problem:

$$531 \quad (\delta s_n^{l+1})_{i,j} = \arg \min_{w_{i,j}} \|[\delta s_n^l - \varrho \mathcal{F}(\delta s_n^l)]_{i,j} - w_{i,j}\|^2,$$

532 subject to $w_{i,j} \leq \kappa - \kappa_0 - (s_{n-1})_{i,j}$ for $i, j = 0, 1, 2, \dots, N_S$. That is,

$$533 \quad (3.34) \quad (\delta s_n^{l+1})_{i,j} = \begin{cases} [\delta s_n^l - \varrho \mathcal{F}(\delta s_n^l)]_{i,j}, & [\delta s_n^l - \varrho \mathcal{F}(\delta s_n^l)]_{i,j} \leq \kappa - \kappa_0 - (s_{n-1})_{i,j}, \\ \kappa - \kappa_0 - (s_{n-1})_{i,j}, & [\delta s_n^l - \varrho \mathcal{F}(\delta s_n^l)]_{i,j} > \kappa - \kappa_0 - (s_{n-1})_{i,j}, \end{cases}$$

534 for $i, j = 0, 1, 2, \dots, N_S$.

535 To summarize the above details, an ADM algorithm for solving (3.1) is listed in Algo-
536 rithm 3.1. Furthermore, based on Algorithm 3.1, we propose Algorithm 3.2 to implement
537 the multiscale approach (2.1)-(2.2), which will be refined later from the viewpoint of the
538 multi-resolution.

Algorithm 3.1 ADM for (3.1)

Initialization: $k = 0$, $\mathbf{u}_n^0 = \mathbf{0}$, $\mathbf{v}_n^0 = \mathbf{0}$, $m_n^0 = 0$, $s_n^0 = 0$, Ω and maximum iteration times K .

while $k \leq K$ **do**

Step 1. Update \mathbf{v}_n^{k+1} by (3.27);

Step 2. Update \mathbf{u}_n^{k+1} by (3.28);

Step 3. Update δm_n^{k+1} by (3.31);

Step 4. Update δs_n^{k+1} by (3.34);

Set $k = k + 1$;

end while

Output: $\mathbf{u}_n = \mathbf{u}_n^K$, $\mathbf{v}_n = \mathbf{v}_n^K$, $\delta m_n = \delta m_n^K$, $\delta s_n = \delta s_n^K$.

Algorithm 3.2 Multiscale algorithm for (2.1)-(2.2)

Initialization: $n = 0$, $\mathbf{u}_n^0 = \mathbf{0}$, $\mathbf{v}_n^0 = \mathbf{0}$, $\delta m_n^0 = 0$, $\delta s_n^0 = 0$, λ_n , θ_n ($n = 0, 1, 2, \dots, N$), Θ and maximum scale N .

while the scale number $n \leq N$ **do**

Step 1. Use Algorithm 3.1 to compute \mathbf{v}_n (cf. (3.27)), \mathbf{u}_n (cf. (3.28)), δm_n (cf. (3.31)) and δs_n (cf. (3.34)) on Ω ;

Step 2. Compute $\tilde{\varphi}_n$, m_n and s_n on Ω ;

Set $n = n + 1$ and go to the next scale with a different value for λ_n (multiscale for parameter λ_n);

end while

Output: $\tilde{\varphi}_N$, m_N , s_N .

539 **4. Coarse-to-fine strategy for the multiscale approach.** To solve the multiscale approach
540 (2.1)-(2.2), one needs to iteratively solve the subproblems (3.3)-(3.6) for each scale n (See

541 Algorithm 3.2 for details). This strategy is not yet efficient. Based on the viewpoint of
 542 the multi-resolution, we now propose a modified coarse-to-fine strategy for the numerical
 543 implementation of the multiscale approach (2.1)-(2.2). This strategy contains following two
 544 steps (the flow chart of the proposed coarse-to-fine strategy is displayed in Fig 5. Note that
 545 here and in what follows, $\Omega \downarrow 2^n$ denotes the downsampling of the region Ω with size 2^n . For
 546 example, given the region $\Omega = (0, 128) \times (0, 128)$, $\Omega \downarrow 2^1$ denotes the region $(0, 64) \times (0, 64)$):

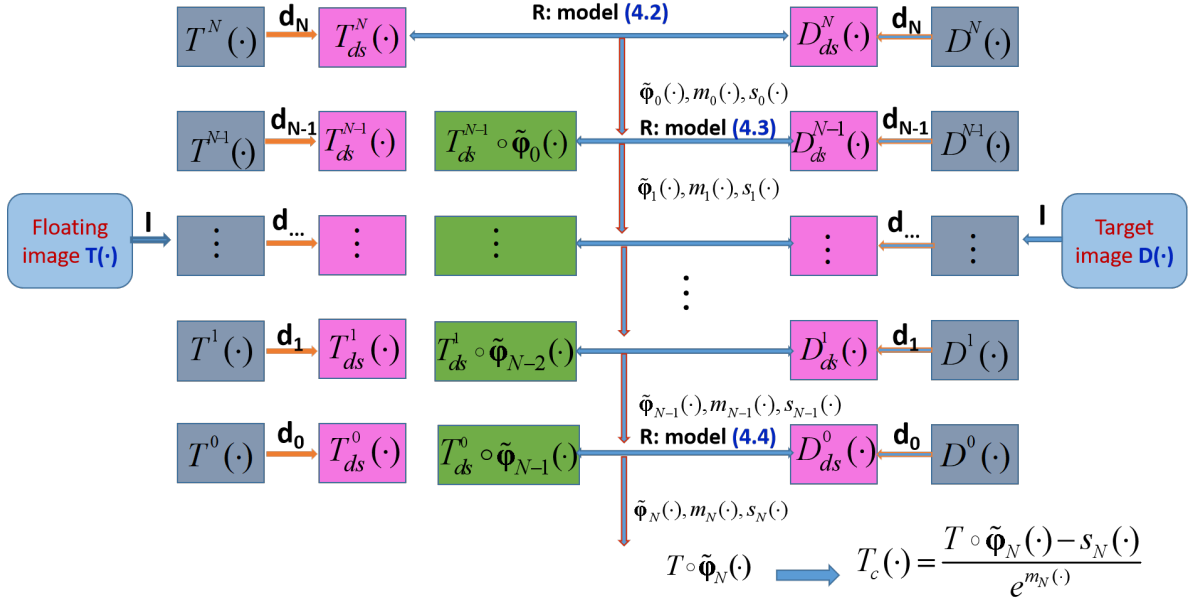


Figure 5. The flow chart of the proposed coarse-to-fine strategy for the joint diffeomorphic image registration and intensity correction. Note that here \mathbf{I} denotes the image decomposition process; \mathbf{R} denotes the image registration process; \mathbf{d} denotes the downsampling process.

547 **(I) Image decomposition:** To improve the resolution of downsampled images, image
 548 decomposition process is additionally introduced. Here, the decomposition model we used is
 549 the canonical multiscale image decomposition model developed by [32,35], which is essentially
 550 based on the following definite partial differential equation (PDE) problem:

$$(4.1) \quad \begin{cases} \frac{\partial \xi(\mathbf{x}, t)}{\partial t} = \rho(t) \operatorname{div} \left(\frac{\delta(\mathbf{x}) \nabla \xi(\mathbf{x}, t)}{|\nabla \xi(\mathbf{x}, t)|} \right), & \mathbf{x} \in \Omega, t > 0, \\ \xi(\mathbf{x}, 0) = f(\mathbf{x}), & \mathbf{x} \in \bar{\Omega}, \\ \xi(\mathbf{x}, t) |_{\mathbf{x} \in \partial \Omega} = 0, & t > 0, \end{cases}$$

552 where we set $\rho(t) = 1.05^t$, $\delta(\mathbf{x}) = \frac{1}{\sqrt{1 + |\nabla(G_\iota * f)(\mathbf{x})|^2 / \beta^2}}$, $\beta = 0.07$ and G_ι is a Gaussian kernel
 553 with a small standard deviation ι . By choosing $N + 1$ different time points $0 = t_0 < t_1 <$
 554 $\dots < t_N$ and setting $f = T$ or $f = D$, we obtain the image decomposition results: $T^N, T^{N-1},$
 555 \dots, T^0 and D^N, D^{N-1}, \dots, D^0 , respectively. Concerning the numerical implementation of
 556 (4.1), one can refer to [35] for details. Therefore, we downsample the decomposed images

557 $T^n(\cdot), D^n(\cdot)$ ($n = 0, 1, 2, \dots, N$) with size 2^n to obtain the downsampled images $T_{ds}^n(\cdot)$ and
 558 $D_{ds}^n(\cdot)$, respectively.

559 *Remark 4.1.* (4.1) is a multiscale process for image decomposition, which acts as a role of
 560 smoothing image if the image pair $T(\cdot), D(\cdot)$ are of low resolutions. In fact, under the situation
 561 where the image pair $T(\cdot), D(\cdot)$ are of high resolutions, we can omit the image decomposition
 562 and downsample the image pair into image sequences $T^n(\cdot), D^n(\cdot)$ ($n = 0, 1, 2, \dots, N$) directly.

563 **(II) Image registration:** The coarse-to-fine strategy for a multiscale approach of joint
 564 image registration and intensity correction model is divided into the following $N + 1$ steps,
 565 here and in what follows, $\Omega_n = \Omega \downarrow 2^{N-n}$ ($n = 0, 1, 2, \dots, N$):

566 **Step 0.** By taking $T_{ds}^N(\cdot)$ and $D_{ds}^N(\cdot)$ as the floating image and target image, respectively,
 567 we solve the following variational problem on Ω_0 :

$$568 \quad (4.2) \quad (\mathbf{u}_0, \delta m_0, \delta s_0) \in \arg \min_{(\mathbf{u}, m, s) \in \mathcal{L}_{\varepsilon_0}(\Omega_0)} \tilde{J}_0(\mathbf{u}, m, s),$$

569 where $\tilde{J}_0(\mathbf{u}, m, s) = \lambda_0 \int_{\Omega_0} (m(\mathbf{x}) + \ln D_{ds}^N(\mathbf{x}) - \ln(T_{ds}^N(\mathbf{x} + \mathbf{u}(\mathbf{x})) - s(\mathbf{x})))^2 dx + \mu R_{\Omega_0}(\mathbf{u}, m, s)$,
 570 $\mathcal{L}_{\varepsilon_0}(\Omega_0) = (\mathcal{A}(\Omega_0) \setminus \mathcal{B}_{\varepsilon_0}(\Omega_0)) \times \mathcal{C}_{\Omega_0} \times SV_0(\Omega_0)$ and $\varepsilon_0 > 0$. $R_{\Omega_n}(\mathbf{u}, m, s)$ is defined by replacing
 571 Ω with Ω_n in (1.3). Define $\tilde{\varphi}_0(\mathbf{x}) = \varphi_0(\mathbf{x}) = \mathbf{x} + \mathbf{u}_0(\mathbf{x})$, $m_0(\mathbf{x}) = \delta m_0(\mathbf{x})$ and $s_0(\mathbf{x}) = \delta s_0(\mathbf{x})$
 572 for each $\mathbf{x} \in \Omega_0$.

573 **Step 1.** Scale $\tilde{\varphi}_0(\mathbf{x})$, $m_0(\mathbf{x})$ and $s_0(\mathbf{x})$ to Ω_1 and solve the following variational problem
 574 on Ω_1 (note that here $|\Omega_1| = 4|\Omega_0|$):

$$575 \quad (4.3) \quad (\mathbf{u}_1, \delta m_1, \delta s_1) \in \arg \min_{(\mathbf{u}, m_0+m, s_0+s) \in \mathcal{L}_{\varepsilon_1}(\Omega_1)} \tilde{J}_1(\mathbf{u}, m, s),$$

576 where $\tilde{J}_1(\mathbf{u}, m, s) = \lambda_1 \int_{\Omega_1} (m_0(\mathbf{x}) + m(\mathbf{x}) + \ln D_{ds}^{N-1}(\mathbf{x}) - \ln(T_{ds}^{N-1} \circ \tilde{\varphi}_0(\mathbf{x} + \mathbf{u}(\mathbf{x})) - s_0(\mathbf{x}) -$
 577 $s(\mathbf{x})))^2 dx + \mu R_{\Omega_1}(\mathbf{u}, m, s)$, $\mathcal{L}_{\varepsilon_1}(\Omega_1) = (\mathcal{A}(\Omega_1) \setminus \mathcal{B}_{\varepsilon_1}(\Omega_1)) \times \mathcal{C}_{\Omega_1} \times SV_0(\Omega_1)$ and $\varepsilon_1 > 0$. Define
 578 $\varphi_1(\mathbf{x}) = \mathbf{x} + \mathbf{u}_1(\mathbf{x})$, $\tilde{\varphi}_1(\mathbf{x}) = \tilde{\varphi}_0 \circ \varphi_1(\mathbf{x})$, $m_1(\mathbf{x}) = m_0(\mathbf{x}) + \delta m_1(\mathbf{x})$ and $s_1(\mathbf{x}) = s_0(\mathbf{x}) + \delta s_1(\mathbf{x})$
 579 for each $\mathbf{x} \in \Omega_1$.

580 \vdots

581 **Step N .** Scale $\tilde{\varphi}_{N-1}(\mathbf{x})$, $m_{N-1}(\mathbf{x})$ and $s_{N-1}(\mathbf{x})$ to Ω_N and solve the following variational
 582 problem on Ω_N (Note that $\Omega_N = \Omega$):

$$583 \quad (4.4) \quad (\mathbf{u}_N, \delta m_N, \delta s_N) \in \arg \min_{(\mathbf{u}, m_{N-1}+m, s_{N-1}+s) \in \mathcal{L}_{\varepsilon_N}(\Omega_N)} \tilde{J}_N(\mathbf{u}, m, s),$$

584 where $\tilde{J}_N(\mathbf{u}, m, s) = \lambda_n \int_{\Omega_N} (m_{N-1}(\mathbf{x}) + m(\mathbf{x}) + \ln D(\mathbf{x}) - \ln(T \circ \tilde{\varphi}_{N-1}(\mathbf{x} + \mathbf{u}(\mathbf{x})) - s_{N-1}(\mathbf{x}) -$
 585 $s(\mathbf{x})))^2 dx + \mu R_{\Omega_N}(\mathbf{u}, m, s)$, $\mathcal{L}_{\varepsilon_N}(\Omega_N) = (\mathcal{A}(\Omega_N) \setminus \mathcal{B}_{\varepsilon_N}(\Omega_N)) \times \mathcal{C}_{\Omega_N} \times SV_0(\Omega_N)$ and $\varepsilon_N > 0$.
 586 Define $\varphi_N(\mathbf{x}) = \mathbf{x} + \mathbf{u}_N(\mathbf{x})$, $\tilde{\varphi}_N(\mathbf{x}) = \tilde{\varphi}_{N-1} \circ \varphi_N(\mathbf{x})$, $m_N(\mathbf{x}) = m_{N-1}(\mathbf{x}) + \delta m_N(\mathbf{x})$ and
 587 $s_N(\mathbf{x}) = s_{N-1}(\mathbf{x}) + \delta s_N(\mathbf{x})$.

588 To show the convergence of the above proposed coarse-to-fine strategy, we introduce some
 589 notations. In the coarse-to-fine strategy, one needs to scale the functions $\varphi^{\Omega_n} : \Omega_n \rightarrow \Omega_n$,
 590 $m^{\Omega_n} : \Omega_n \rightarrow \mathbb{R}$, $s^{\Omega_n} : \Omega_n \rightarrow \mathbb{R}$ and $\mathbf{u}^{\Omega_n} : \Omega_n \rightarrow \mathbb{R}$ to the functions $\varphi : \Omega \rightarrow \Omega$, $m : \Omega \rightarrow \mathbb{R}$,

591 $s : \Omega \rightarrow \mathbb{R}$ and $\mathbf{u} : \Omega \rightarrow \mathbb{R}$, respectively. By the principle of scaling, there holds $\varphi(\mathbf{y}) =$
 592 $2^{N-n}\varphi^{\Omega_n}(\frac{\mathbf{y}}{2^{N-n}})$, $\mathbf{u}(\mathbf{y}) = 2^{N-n}\mathbf{u}^{\Omega_n}(\frac{\mathbf{y}}{2^{N-n}})$, $m(\mathbf{y}) = m^{\Omega_n}(\frac{\mathbf{y}}{2^{N-n}})$, and $s(\mathbf{y}) = s^{\Omega_n}(\frac{\mathbf{y}}{2^{N-n}})$, where
 593 $\mathbf{y} \in \Omega$ and $\mathbf{x} = \mathbf{y}/2^{N-n} \in \Omega_n$. Here, functions f_{Ω_n} ($f = \varphi, m, s, \mathbf{u}$) denote the version
 594 of the function f on the domain Ω_n . In addition, there also holds $T_{ds}^n(\frac{\mathbf{y}}{2^{N-n}}) = T(\mathbf{y})$ and
 595 $D_{ds}^n(\frac{\mathbf{y}}{2^{N-n}}) = D(\mathbf{y})$.

596 Based on these notations, we have the following results.

597 **Theorem 4.2.** *For any $n \leq N - 1$, the coarse level registration problem*

$$598 \quad (4.5) \quad (\mathbf{u}_n^{\Omega_n}, \delta m_n^{\Omega_n}, \delta s_n^{\Omega_n}) \in \arg \min_{(\mathbf{u}^{\Omega_n}, m^{\Omega_n-1} + m^{\Omega_n}, s^{\Omega_n-1} + s^{\Omega_n}) \in \mathcal{L}_{\varepsilon_n}(\Omega_n)} \tilde{E}_n(\mathbf{u}^{\Omega_n}, m^{\Omega_n}, s^{\Omega_n})$$

599 *is equivalent to the following variational problem*

$$600 \quad (4.6) \quad (\mathbf{u}_n, \delta m_n, \delta s_n) \in \arg \min_{(\mathbf{u}, m_n + m, s_n + s) \in \mathcal{L}_{\varepsilon_n}(\Omega)} \bar{E}_n(\mathbf{u}, m, s),$$

601 where $\tilde{E}_n(\mathbf{u}, m, s) = \lambda_n \int_{\Omega_n} (m_{n-1}^{\Omega_n}(\mathbf{x}) + m^{\Omega_n}(\mathbf{x}) + \ln D_{ds}^{N-n}(\mathbf{x}) - \ln(T_{ds}^{N-n} \circ \tilde{\varphi}_{n-1}^{\Omega_n}(\mathbf{x} + \mathbf{u}^{\Omega_n}(\mathbf{x})) -$
 602 $s_{n-1}^{\Omega_n}(\mathbf{x}) - s^{\Omega_n}(\mathbf{x})))^2 d\mathbf{x} + \mu R_{\Omega_n}(\mathbf{u}^{\Omega_n}, m^{\Omega_n}, s^{\Omega_n})$, $\bar{E}_n(\mathbf{u}, m, s) = 4^{N-n} \lambda_n \int_{\Omega} (m_{n-1}(\mathbf{x}) + m(\mathbf{x}) +$
 603 $\ln D_{ds}^{N-n}(\mathbf{x}) - \ln(T_{ds}^{N-n} \circ \tilde{\varphi}_{n-1}(\mathbf{x} + \mathbf{u}(\mathbf{x})) - s_{n-1}(\mathbf{x}) - s(\mathbf{x})))^2 d\mathbf{x} + \mu(R_{1,\Omega}(\mathbf{u}) + 2^{N-n}(R_{2,\Omega}(m) +$
 604 $R_{3,\Omega}(s)))$.

605 *Proof.* By letting $\mathbf{y} = 2^{N-n}\mathbf{x} \in \Omega$ for any $\mathbf{x} \in \Omega_n$, we get

$$606 \quad \begin{aligned} & \tilde{E}_n(\mathbf{u}^{\Omega_n}, m^{\Omega_n}, s^{\Omega_n}) \\ &= \frac{1}{4^{N-n}} \lambda_n \int_{\Omega} (m_{n-1}(\mathbf{y}) + m(\mathbf{y}) + \ln D_{ds}^{N-n}(\mathbf{y}) - \ln(T_{ds}^{N-n} \circ \tilde{\varphi}_{n-1}(\mathbf{y} + \mathbf{u}(\mathbf{y}))) \\ & \quad - s_{n-1}(\mathbf{y}) - s(\mathbf{y})))^2 d\mathbf{y} + \frac{\mu}{16^{N-n}} (R_{1,\Omega}(\mathbf{u}) + 2^{N-n}(R_{2,\Omega}(m) + R_{3,\Omega}(s))). \end{aligned}$$

607 Therefore, (4.5) is equivalent to (4.6). ■

608 By Theorem 4.2, the variational problem (4.2)-(4.4) on each coarse grid is equivalent to
 609 the following variational problem

$$610 \quad (4.7) \quad (\mathbf{u}_n, \delta m_n, \delta s_n) \in \arg \min_{(\mathbf{u}, m_{n-1} + m, s_{n-1} + s) \in \mathcal{L}_{\varepsilon_n}(\Omega)} \bar{E}_n(\mathbf{u}, m, s), \quad n = 0, 1, 2, \dots, N.$$

611 Then based on Theorems 4.2 and 2.6, we give the following convergence result of the proposed
 612 coarse-to-fine strategy (4.2)-(4.4).

613 **Theorem 4.3.** *Let $\tilde{\varphi}_n$ and m_n, s_n ($n = 0, 1, 2, \dots, N$) be induced by the multiscale approach*
 614 *(4.2)-(4.4). Assume three large numbers B, M, λ_n satisfy $\lim_{n \rightarrow N^-, N \rightarrow +\infty} \frac{B^{4n-3} M^{4^n}}{\lambda_n} = 0$, where*
 615 *B is a positive number depending on Ω and M is a positive number depending on $\mathbf{u}_0, \delta m_0,$*
 616 *$\delta s_0, \Omega, \alpha$ and ϕ , respectively. Then there holds $\phi = \delta$, i.e., the modified coarse to fine strategy*
 617 *(4.2)-(4.4) is also equivalent to the original greedy matching problem (2.17).*

618 *Proof.* Based on Theorem 4.2, we can transform the variational problems (4.2)-(4.4) into
 619 an equivalent problem (4.7), which is defined on Ω . Further, one can notice that (4.7) is
 620 equivalent to (2.2) with $n \rightarrow N^-$. Therefore, we can use Theorem 2.6 to show $\phi = \delta$. ■

Algorithm 4.1 Coarse-to-fine algorithm for the multiscale approach (4.2)-(4.4)

Initialization: $n = 0$, $\mathbf{u}_n^0 = \mathbf{0}$, $\mathbf{v}_n^0 = \mathbf{0}$, $m_n^0 = 0$, $s_n^0 = 0$, λ_n , θ_n ($n = 0, 1, 2, \dots, N$), Θ and maximum scale N .

I: Image decomposition:

Solve the image decomposition model (4.1) by setting $f = T$ and D to obtain the decomposition result; Downsample the decomposed images T^n, D^n ($n = 0, 1, 2, \dots, N$) with size 2^n to obtain the downsampled images $T_{ds}^n(\cdot)$ and $D_{ds}^n(\cdot)$, respectively.

II: Image registration:

while $n < N$ **do**

Step 1. Use Algorithm 3.1 to compute \mathbf{v}_n (cf. (3.27)), \mathbf{u}_n (cf. (3.28)), δm_n (cf. (3.31)) and δs_n (cf. (3.34)) on Ω_n and replace $T(\cdot), D(\cdot)$ with $T_{sd}^{N-n}(\cdot), D_{sd}^{N-n}(\cdot)$, respectively;

Step 2. Compute $\tilde{\varphi}_n, m_n$ and s_n on Ω_n ;

Step 3. Scale the definition of $\tilde{\varphi}_n, m_n$ and s_n onto a finer domain Ω_{n+1} ;

Set $n = n + 1$;

end while

Output: $\tilde{\varphi}_{N,m_N}, s_N$ and $T_c(\cdot) = \frac{T \circ \tilde{\varphi}_N(\cdot) - s_N(\cdot)}{e^{m_N(\cdot)}}$.

621 Based on Algorithm 3.1, the proposed coarse-to-fine strategy for the multiscale approach
622 (4.2)-(4.4) is summarized in Algorithm 4.1.

623 *Remark 4.4.* Algorithm 4.1 is a multi-resolution modification for Algorithm 3.2. In Al-
624 gorithm 3.2, we need to solve the variational problem on Ω , while in Algorithm 4.1, we just
625 need to solve the same problem on Ω_n ($n = 0, 1, 2, \dots, N$). By $|\Omega_n| = \frac{1}{4^{N-n}}|\Omega|$, we know that
626 Algorithm 4.1 accelerates Algorithm 3.2, which will be validated in Section 5. In addition, by
627 Theorem 4.2, the scale n of the coarse-to-fine approach (4.2)-(4.4) is equivalent to the scale n
628 of the non-coarse-to-fine approach (4.7), whatever the region Ω is downsampled. Hence, the
629 downsampling process does not affect the final result when n is large enough.

630 **5. Applications for the proposed multiscale approach.** In this section, we perform three
631 different kinds of numerical tests to validate the theoretical results and algorithms in Section
632 2-4. The content of this section contains: In Test 5.2, we perform the comparison between the
633 proposed coarse-to-fine Algorithm 4.1 and M2FDIR in [21] to show that Algorithm 4.1 is more
634 efficient on addressing the image registration problem with local varying illumination. In Test
635 5.3, a comparison between Algorithm 4.1 and Algorithm 3.2 is performed to show that the
636 proposed Algorithm 4.1 has advantage on reducing the CPU consumption. In Test 5.4, the
637 proposed Algorithm 4.1 is compared with some state-of-the-art image registration algorithms,
638 including 1DFDIM [18], DFIRA [19], LDDMM [25] and FBNE [33]. All the numerical tests
639 are performed under Windows 7 and MATLAB R2012b with Intel core i7-6700 CPU @3.40
640 GHz and 8GB memory. For the quantitative comparison, we choose the following two indices:

- Relative sum of squared differences (Re-SSD for short) defined by

$$642 \quad \text{Re-SSD}(T, D, \mathbf{u}) = \frac{\text{SSD}(T(\mathbf{x} + \mathbf{u}), D)}{\text{SSD}(T, D)},$$

643 where $\text{SSD}(T, D) = \frac{1}{2} \sum_{i,j} (T_{i,j} - D_{i,j})^2$;

644 • Mesh folding number (MFN for short) defined by

645
$$\text{MFN}(\mathbf{u}) = \#(\det \bar{J}(\mathbf{u}) \leq 0),$$

646 where $\det \bar{J}(\mathbf{u}) = \left(1 + \frac{\partial u_1}{\partial x_1}\right) \left(1 + \frac{\partial u_2}{\partial x_2}\right) - \frac{\partial u_1}{\partial x_2} \frac{\partial u_2}{\partial x_1}$ and for any set A , $\#(A)$ denotes the
647 number of elements in A .

648 **5.1. Sensitivity test for parameters λ_n and μ in Algorithm 4.1.** λ_n and μ are two key
649 parameters for Algorithm 4.1. To show the sensitivity of the sequence $\{\lambda_n\}$ and the parameter
650 μ , the synthetic image pair (pair I) is used as the testing data. For pair I, the floating image
651 and target image are defined as follows:

652
$$T(\mathbf{x}) = 255\chi_{\bar{\Gamma}_1}(\mathbf{x}) + 0.01, \quad D(\mathbf{x}) = 255\chi_{\bar{\Gamma}_2}(\mathbf{x}) + 100\chi_{\bar{\Gamma}_3}(\mathbf{x}) + 0.01,$$

653 where $\Omega = (0, 128) \times (0, 128)$, $\bar{\Gamma}_1 = \{\mathbf{x} = (x_1, x_2)^T : (x_1 - 65)^2 + (x_2 - 65)^2 \leq 40^2\}$, $\bar{\Gamma}_2 =$
654 $\{\mathbf{x} = (x_1, x_2)^T : (x_1 - 65)^2 + (x_2 - 65)^2 < 10^2\}$, $\bar{\Gamma}_3 = \{\mathbf{x} = (x_1, x_2)^T : 10^2 \leq (x_1 - 65)^2 +$
655 $(x_2 - 65)^2 \leq 20^2\}$ and χ is an indicator function. The original synthetic image pair is shown
656 in Fig 7.

657 By setting $\lambda_n = \lambda_0 \times 4^n (n = 0, 1, 2, \dots)$, $\mu \in [0.01, 1000]$ and $\lambda_0 \in [15000, 100000]$, we use
658 Algorithm 4.1 to perform the registration for image pair I by giving 357 different groups (only
659 132 groups are shown on Fig 6 to make the vision more plausible) of λ_0 and μ . By viewing
660 the final $\text{Re_SSD}(T, D, \mathbf{u})$ as the heat value, the heat map for λ_0 and μ is shown in Fig 6.

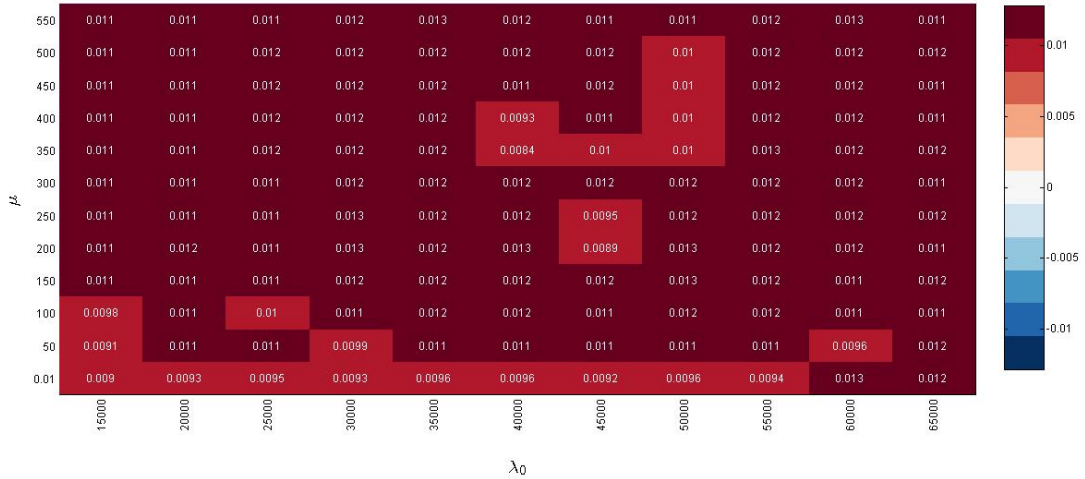


Figure 6. The heat map for λ_0 and μ . The values in the table are $\text{Re_SSD}(T, D, \mathbf{u})$ with respect to different λ_0 and μ .

661 According to Fig 6, we find that the final $\text{Re_SSD}(T, D, \mathbf{u})$ is not affected by the parameters

662 λ_n and μ . This validates that the multiscale approach (2.1)-(2.2) can provide a solution to
 663 the greedy matching problem (2.17), which has nothing to do with the parameters λ_n and μ .

664 **5.2. Comparison between the proposed coarse-to-fine Algorithm 4.1 and M2FDIR**
 665 **in [21].** To show that the proposed model via (4.2)-(4.4) properly treats the local varying
 666 illumination, we compare the proposed Algorithm 4.1 with the multiscale M2FDIR in [21],
 667 which does not take the local varying illumination into consideration. The test pair in this
 668 part contains synthetic image pair I and two brain MRI image pairs (II-III) with local varying
 669 illumination.

670 For pair I, one can notice from Fig 7 that there is a shadow on the outer ring of the
 671 circle in the target image $D(\cdot)$, while no shadow appears in the floating image $T(\cdot)$. By using
 672 image pair I, we use the proposed Algorithm 4.1 and M2FDIR in [21] for registration. The
 673 final registration results and quantitative comparison are listed in Fig 7 and Table 1. By Fig
 674 7(f), one can notice that the proposed Algorithm 4.1 produces a diffeomorphic deformation
 675 φ . It follows from Fig 7(d) that the registration result of Algorithm 4.1 matches the shadow
 676 ring of the target image $D(\cdot)$ well, while the final result of M2FDIR has trouble in matching
 677 the shadow ring. Besides, M2FDIR leads to a wrong result because of the distortion of
 678 the shadow ring in target image $D(\cdot)$. This shows the necessity to introduce the bias m, s
 679 in variational model (1.3), and also validate that the proposed Algorithm 4.1 addresses the
 680 image registration with local illumination well.

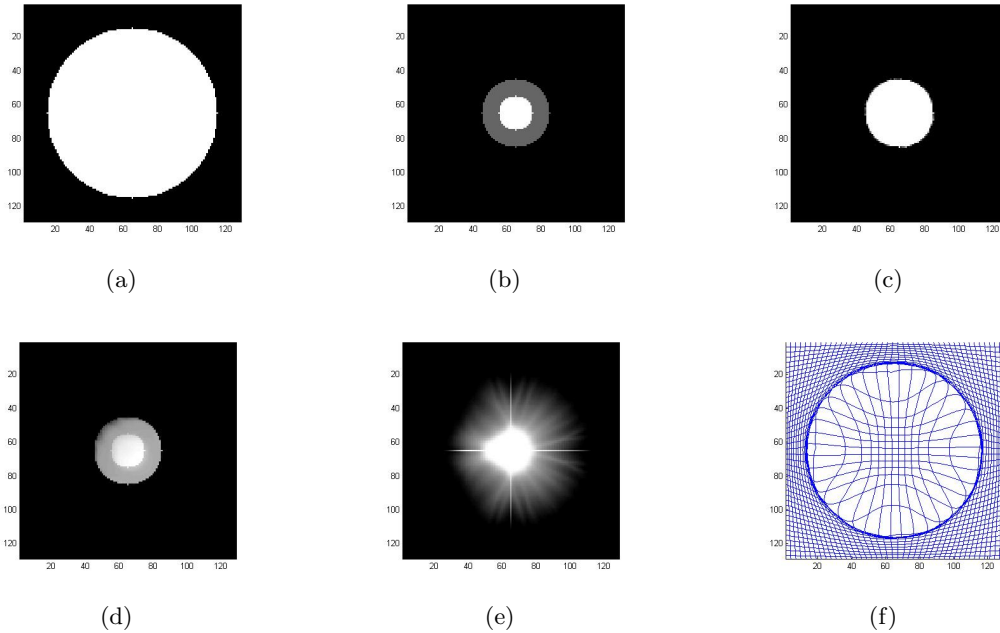


Figure 7. Comparison on pair I: (a) floating image $T(\cdot)$; (b) target image $D(\cdot)$; (c) $T \circ \tilde{\varphi}_N(\cdot)$ in Algorithm 4.1, $\text{Re.SSD}=5.14\%$; (d) $T_c \circ \tilde{\varphi}_N(\cdot)$ in Algorithm 4.1, $\text{Re.SSD}=0.89\%$; (e) $T \circ \tilde{\varphi}_{KM}(\cdot)$ in M2FDIR [21], $\text{Re.SSD}=7.65\%$; (f) mesh grid of the deformation $\tilde{\varphi}_N(\cdot)$ in Algorithm 4.1

681 For pair II (see the first row of Fig 8), there are two domains suffering from local varying
 682 illumination on the lower left of the floating image $T(\cdot)$, while no illumination appears in the

Table 1
Quantitative comparison between registration results of Algorithm 4.1 and M2FDIR (Test 5.2)

Data	Algorithm	Re-SSD(%)	MFN	CPU/s
Pair I	M2FDIR [21]	7.65	0	469.3
	Algorithm 4.1	0.89	0	37.1
Pair II	M2FDIR [21]	46.86	0	536.1
	Algorithm 4.1	11.82	0	36.1
Pair III	M2FDIR [21]	9.91	0	661.3
	Algorithm 4.1	3.11	0	43.1

683 target image $D(\cdot)$. For pair III (see the second row of Fig 8), there is local illumination on
 684 the right side of the floating image $T(\cdot)$, while local illumination appears on the opposite side
 685 of the target image $D(\cdot)$. We use Algorithm 4.1 and M2FDIR for pairs II and III. The results
 686 are shown in Fig 8 and the quantitative comparison result are listed in Table 1.

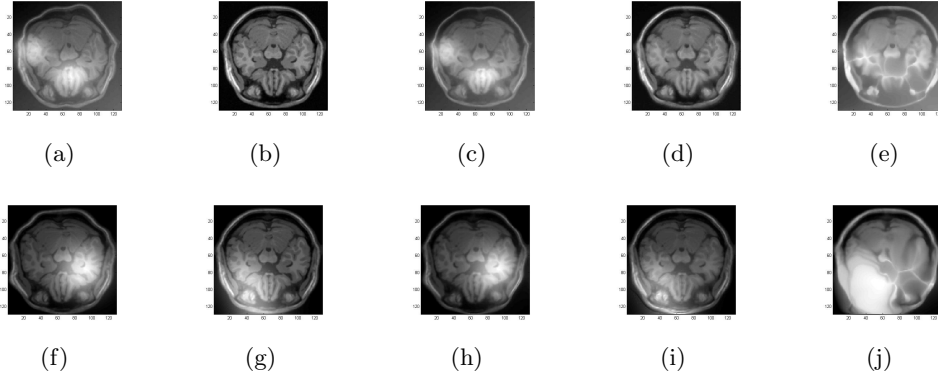


Figure 8. Comparison on pair II (First row): (a) floating image $T(\cdot)$; (b) target image $D(\cdot)$; (c) $T \circ \tilde{\varphi}_N(\cdot)$ in Algorithm 4.1, Re_SSD=85.31%; (d) $T_c \circ \tilde{\varphi}_N(\cdot)$ in Algorithm 4.1, Re_SSD=11.82%; (e) $T \circ \tilde{\varphi}_{KM}(\cdot)$ in M2FDIR [21], Re_SSD=46.86%. Comparison on pair III (Second row): (f) floating image $T(\cdot)$; (g) target image $D(\cdot)$; (h) $T \circ \tilde{\varphi}_N(\cdot)$ in Algorithm 4.1, Re_SSD=86.04%; (i) $T_c \circ \tilde{\varphi}_N(\cdot)$ in Algorithm 4.1, Re_SSD=3.11%; (j) $T \circ \tilde{\varphi}_{KM}(\cdot)$ in M2FDIR [21], Re_SSD=9.91%;

687 By Fig 8(e), we see that the registration result of M2FDIR on pair II is disturbed by the
 688 local varying illumination and leads to an unexpected result. In addition, one can notice from
 689 Fig 8(d) that the proposed Algorithm 4.1 addresses the local varying illumination well. This
 690 validates that the proposed Algorithm 4.1 has advantage on addressing the registration with
 691 local varying illumination over M2FDIR, which is also the main motivation for us to study
 692 the problem joint diffeomorphic image registration and intensity correction. Concerning the
 693 comparison on pair III, it follows from Fig 8(j) that the registration result is seriously bad in
 694 the region with local varying illumination, while the proposed Algorithm 4.1 can accurately
 695 correct the intensity distortion caused by the local illumination (see Fig 8(i) for details). In
 696 addition, in pair II and III, one can notice that the final Re_SSD of M2FDIR is smaller than
 697 the Re_SSD ($T \circ \tilde{\varphi}_N(\cdot)$ in Algorithm 4.1) before intensity correction. This improvement in
 698 Re_SSD is meaningless since the pursuit of a smaller Re_SSD leads to a wrong deformation

699 (seriously bad in the local illumination region). Lastly, one can notice from the registration
 700 result of Algorithm 4.1 (Fig 8(f)-(j)) that there is still local varying illumination to coincide
 701 with the target image. That is, local varying illumination still can not be recovered well if
 702 there is local varying illumination in target image $D(\cdot)$. This validates the fact in Remark
 703 1.3 that the fidelity in (1.3) is formulated based on the assumption that the target image $D(\cdot)$
 704 has no bias.

705 **5.3. Comparison between the proposed coarse-to-fine Algorithm 4.1 and Algorithm**
 706 **3.2 (without coarse-to-fine process).** To solve the proposed multiscale approach (2.1)-(2.2),
 707 one has two choices: (1) Use the proposed Algorithm 3.2 without coarse-to-fine strategy. For
 708 this choice, one is expected to implement the ADM process (4.2)-(4.4) on Ω for each scale
 709 n . (2) Use the proposed coarse-to-fine Algorithm 4.1. For this choice, one only needs to
 710 solve the ADM process (4.2)-(4.4) on Ω_n for each scale n . Note that Ω_n is a domain smaller
 711 than Ω , which indicates that the proposed coarse-to-fine strategy (4.2)-(4.4) has advantage
 712 on reducing the CPU consumption over Algorithm 3.2.

713 To numerically validate this theoretical result, we perform the comparison between Algo-
 714 rithm 4.1 and Algorithm 3.2. Both two algorithms aim to find the solution of the multiscale
 715 approach (2.1)-(2.2), where the coarse-to-fine strategy is introduced in Algorithm 4.1, but no
 716 multi-resolution based coarse-to-fine strategy is used in Algorithm 3.2. The data set used
 717 for the test are labelled IV-VI. For pair IV, it contains five image pairs which are collected
 718 at two different time from one patient (No.1) who suffers from the mouth cavity lymphoma.
 719 Similarly, data V and VI contain the same content from other two patients (No.2 and No.3).
 720 By registering these image pairs, clinicians can extract useful information from the difference
 721 between the deformed image $T_c \circ \tilde{\varphi}_N(\cdot)$ and the target image $D(\cdot)$. Furthermore, by analyzing
 722 the difference, some evaluation for the severeness of the tumor is made. Therefore, the accu-
 723 racy of the image registration result is of vital importance for the evaluation. Here, we use
 724 Algorithm 4.1 and Algorithm 3.2 to register these 15 image pairs. The registration results for
 725 IV-VI are listed on Fig 9-11 and Table 2, where Re_SSD is represented by the mean value \pm
 726 standard deviation of five different image pairs for each patient, and the CPU is represented
 727 in a similar way.

Table 2

Quantitative comparison between registration results of Algorithm 4.1 and Algorithm 3.2 (Test 5.3)

Data	Algorithm	Re-SSD(%)	MFN	CPU/s
data IV	Algorithm 4.1	10.67 ± 2.47	0	38.5 ± 5.3
	Algorithm 3.2	11.19 ± 3.44	0	518.5 ± 31.9
data V	Algorithm 4.1	9.82 ± 2.47	0	36.1 ± 6.1
	Algorithm 3.2	13.16 ± 3.51	0	436.7 ± 35.6
data VI	Algorithm 4.1	8.96 ± 1.68	0	43.1 ± 3.8
	Algorithm 3.2	12.76 ± 0.72	0	621.7 ± 45.6

728 By Table 2, we see that the registration result of the proposed Algorithm 4.1 is similar to
 729 (though a bit better than) Algorithm 3.2. However, the CPU consumption of Algorithm 4.1
 730 is greatly reduced compared with Algorithm 3.2. This shows the efficiency of the proposed

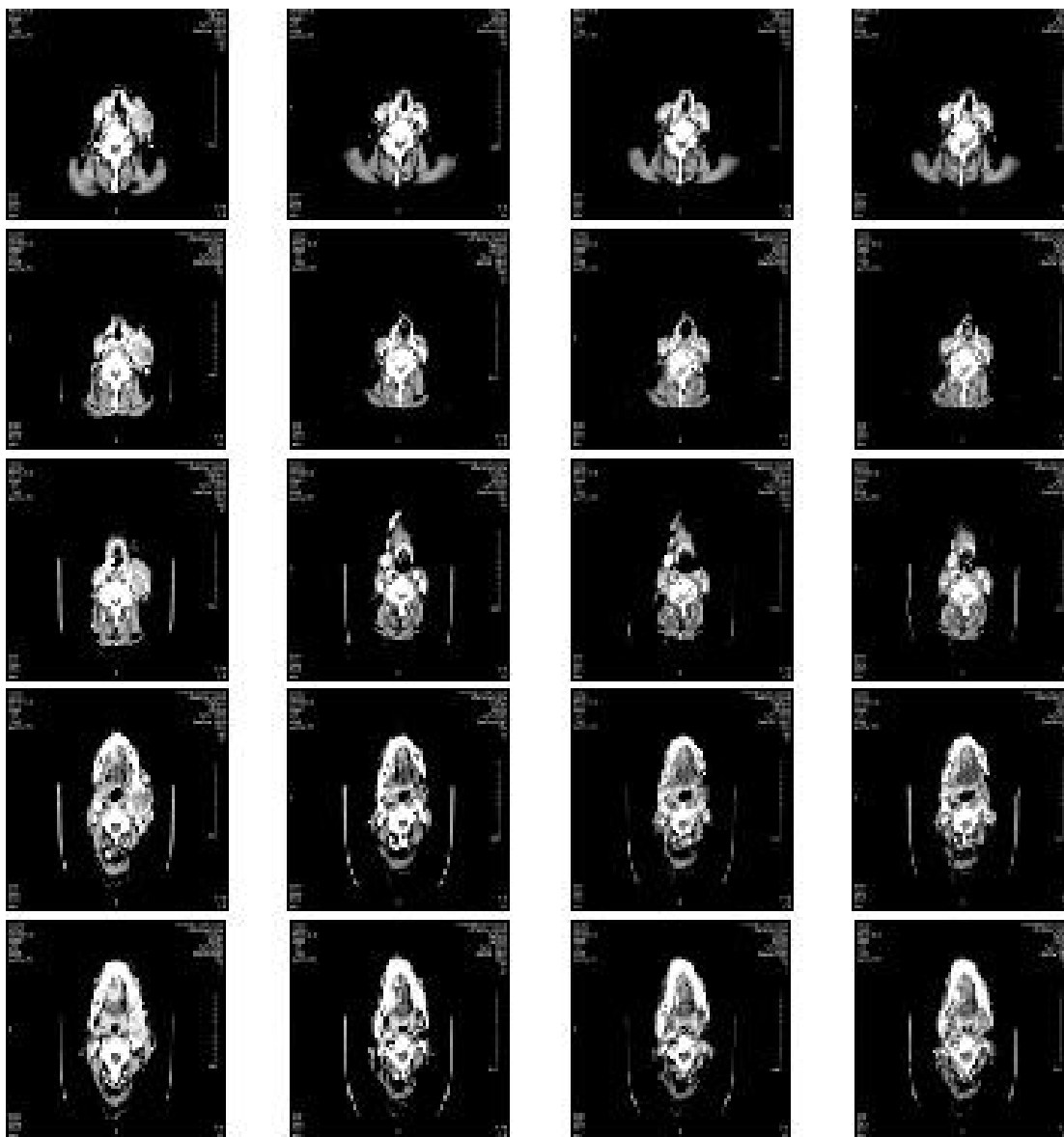


Figure 9. Comparison on IV: The first column is the floating image $T(\cdot)$ for each image pair; The second column is the floating image $D(\cdot)$ for each image pair; The third and fourth columns are the image registration results of Algorithm 4.1 and Algorithm 3.2 for each image pair, respectively.

731 coarse-to-fine Algorithm 4.1.

732 **5.4. Comparison between Algorithm 4.1 and some other image registration algorithms.**

733 In this part, to further validate the effectiveness and efficiency of the proposed coarse-to-
 734 fine Algorithm 4.1, we perform some comparisons between Algorithm 4.1 and 1DFDIM [18],
 735 DFIRA [19], LDDMM [25] and FBNE [33]. For this purpose, we use these five algorithms
 736 to match three different medical image pairs labelled with VII-IX. Here, VII-IX are kept the

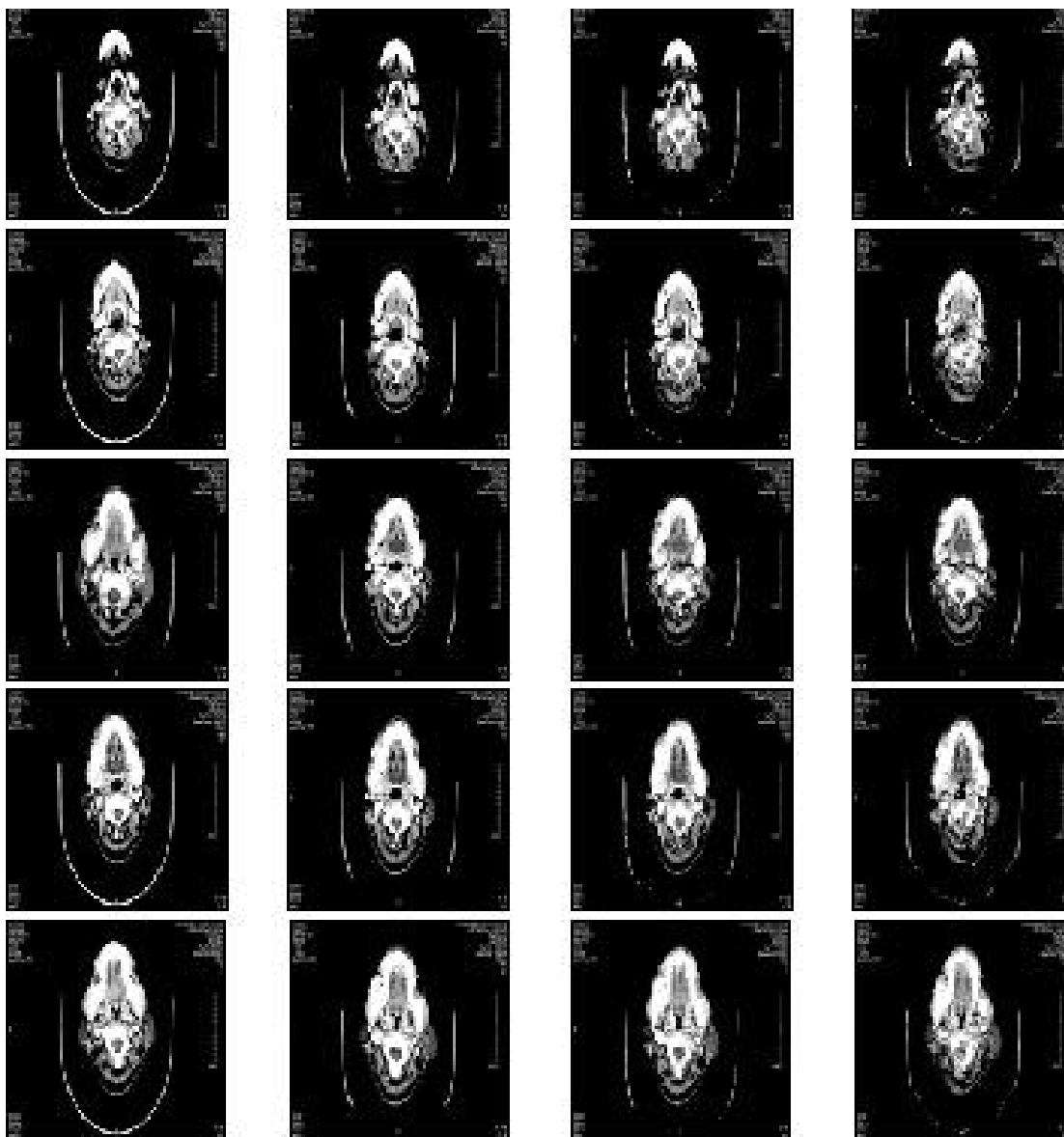


Figure 10. Comparison on V : The first column is the floating image $T(\cdot)$ for each image pair; The second column is the floating image $D(\cdot)$ for each image pair; The third and fourth columns are the image registration results of Algorithm 4.1 and Algorithm 3.2 for each image pair, respectively.

737 same state with data set used in [33], which are introduced as follows.

738 For image pair VII, the floating image $T(\cdot)$ contains a highly contrasted part in the mid-
 739 dle of the region. By viewing the contrast as bias field relative to the target image $D(\cdot)$, the
 740 elimination of this kind of bias field provides a strong evidence that the proposed multiscale
 741 approach for the variational model joint image registration and intensity correction has ad-
 742 vantage on addressing the diffeomorphic registration with local varying illumination. This

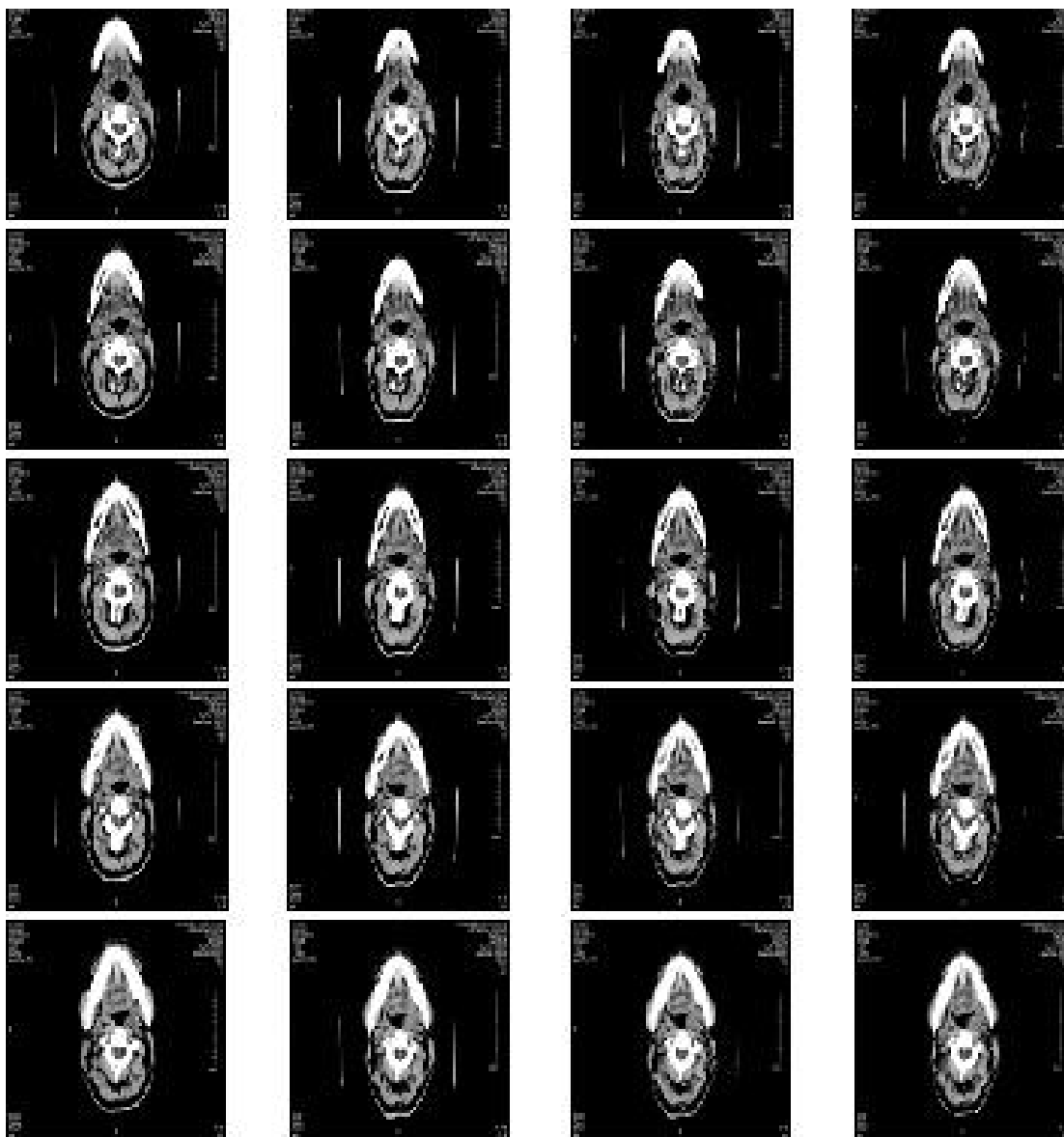


Figure 11. Comparison on VI: The first column is the floating image $T(\cdot)$ for each image pair; The second column is the floating image $D(\cdot)$ for each image pair; The third and fourth columns are the image registration results of Algorithm 4.1 and Algorithm 3.2 for each image pair, respectively.

743 is the main reason why these image pairs are selected for the numerical comparison. The
 744 quantitative comparison results for image pair VII are listed in Fig 12 and Table 3. One can
 745 notice from Fig 12 that only the proposed algorithm and the FBNE in [33] eliminate the bias
 746 field in the middle of the region well. The other three algorithms which do not take intensi-
 747 ty correction into consideration lead to a narrow white bias field. This phenomenon occurs
 748 due to the minimization of the similarity $S(\mathbf{u})$. These solutions are not expected in image

749 registration of image pair VII, which shows that the necessity for introducing the intensity
 750 correction process in the proposed Algorithm 4.1. Note that [33] pursues a minimizer of the
 751 cost functional with three different regularizations, while Algorithm 4.1 searches for the min-
 752 imizer of $S(\mathbf{u}, m, s)$ without any regularization. The comparison between Algorithm 4.1 and
 753 FBNE in [33] further validates the advantage of greedy matching. However, without proper
 754 multiscale consideration, greedy matching without regularization is not expected to work well,
 755 which illustrates that why the multiscale approach is introduced in this paper.

756 For image pairs VIII, there is a low contrast in some local region of the floating image $T(\cdot)$,
 757 which may make it ineffective for some image registration models without intensity correction
 758 process. The registration result for image pair VIII is listed in Fig 13 and Table 3. The
 759 proposed algorithm and FBNE [33] successfully recover the low contrast region and lead to a
 760 final result with more details on the tissue. This shows the importance of intensity correction
 761 in the registration for these image pairs with a low contrast floating image. In this view, it is
 762 helpful to use the proposed algorithm to register the image pairs containing at least one high
 763 resolution image and one low contrast image. In addition, one can notice from Table 3 that
 764 the proposed Algorithm 4.1 achieves the best result for image pair VIII.

765 For image pair IX, the floating image contains bias field and varying illumination on
 766 different regions of the domain. Compared with image pair II used in Test 5.2, there is
 767 a square shadow surrounding the brain, which may affect the registration result. By Fig
 768 14, we see that the local bias and square shadow are well eliminated in the final result of
 769 the proposed Algorithm 4.1 and FBNE. This is an advantage led by bias correction in the
 770 proposed Algorithm 4.1 and FBNE. Moreover, by the quantitative comparisons on Table 3,
 771 one can see that the proposed Algorithm 4.1 achieves a smaller Re_SSD than FBNE.

Table 3

Quantitative comparisons between five different image registration algorithms

Data	Algorithm	Re-SSD(%)	MFN	CPU/s
	Algorithm 4.1	9.76	0	40.3
data VII	1DFDIM [18]	25.72	0	62.7
	DFIRA [19]	22.80	0	372.6
	LDDMM [25]	50.05	0	21.2
	FBNE [33]	12.57	0	118.6
	Algorithm 4.1	5.28	0	42.2
data VIII	1DFDIM [18]	76.09	0	86.3
	DFIRA [19]	66.54	0	456.7
	LDDMM [25]	51.23	0	30.2
	FBNE [33]	24.41	0	101.6
	Algorithm 4.1	3.05	0	50.4
data IX	1DFDIM [18]	83.2	0	90.3
	DFIRA [19]	68.96	0	748.4
	LDDMM [25]	36.18	0	23.7
	FBNE [33]	15.44	0	117.3

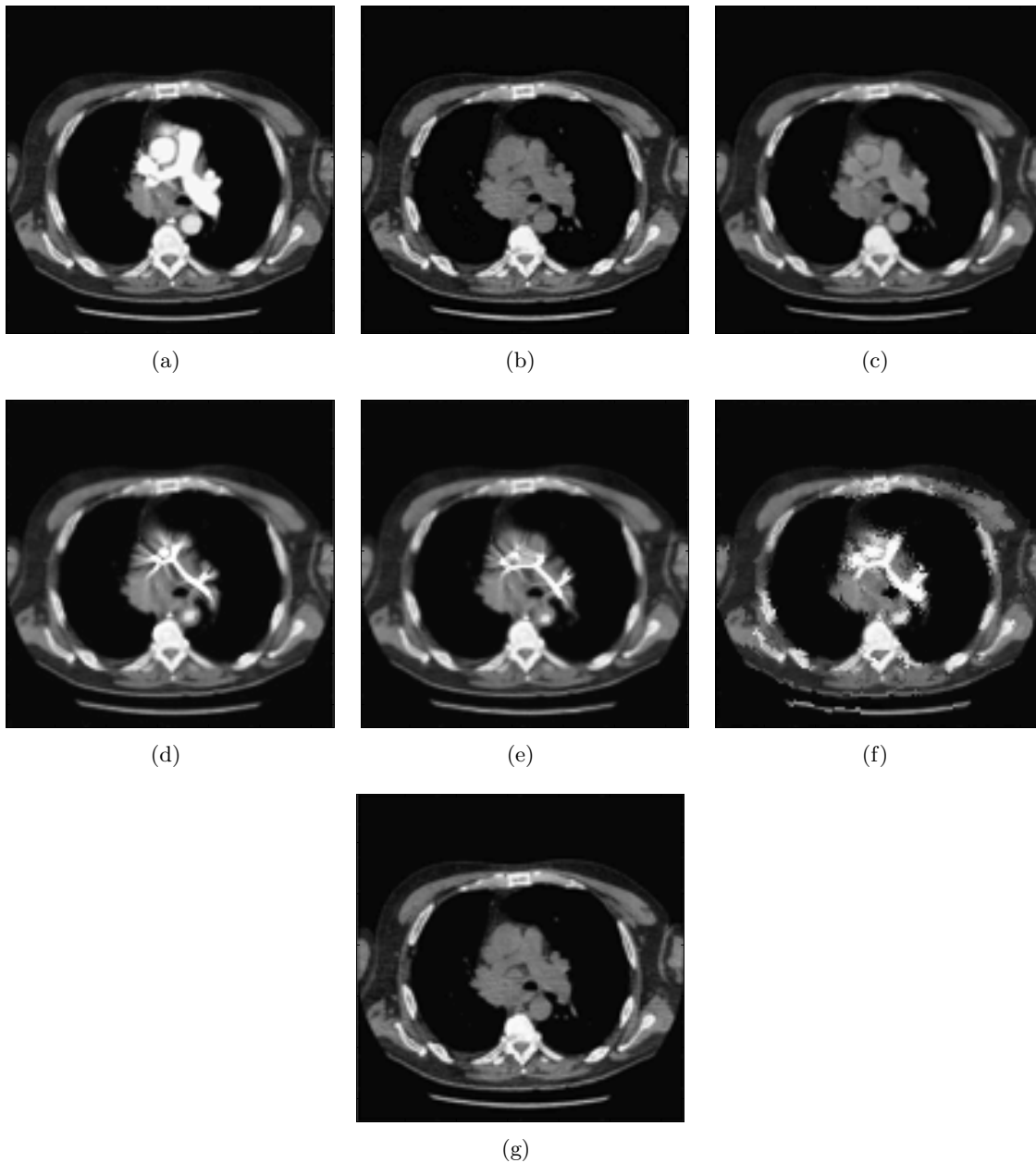


Figure 12. Comparison on VII: (a) floating image $T(\cdot)$; (b) target image $D(\cdot)$; (c) $T \circ \tilde{\varphi}_N(\cdot)$ in Algorithm 4.2, $\text{Re.SSD}=9.76\%$; (d) 1DFDIM, $\text{Re.SSD}=25.72\%$; (e) DFIRA, $\text{Re.SSD}=22.8\%$; (f) LDDMM, $\text{Re.SSD}=50.05\%$; (g) FBNE, $\text{Re.SSD}=12.57\%$.

772 6. Discussion.

773 **6.1. Advantages of the multiscale approach.** To address the intensity inhomogeneity in
 774 image registration, a state-of-the-art model was proposed by Theljani and Chen [33]. Further-
 775 more, by using the Nash game theory, an iterative algorithm (FBNE) is also proposed based

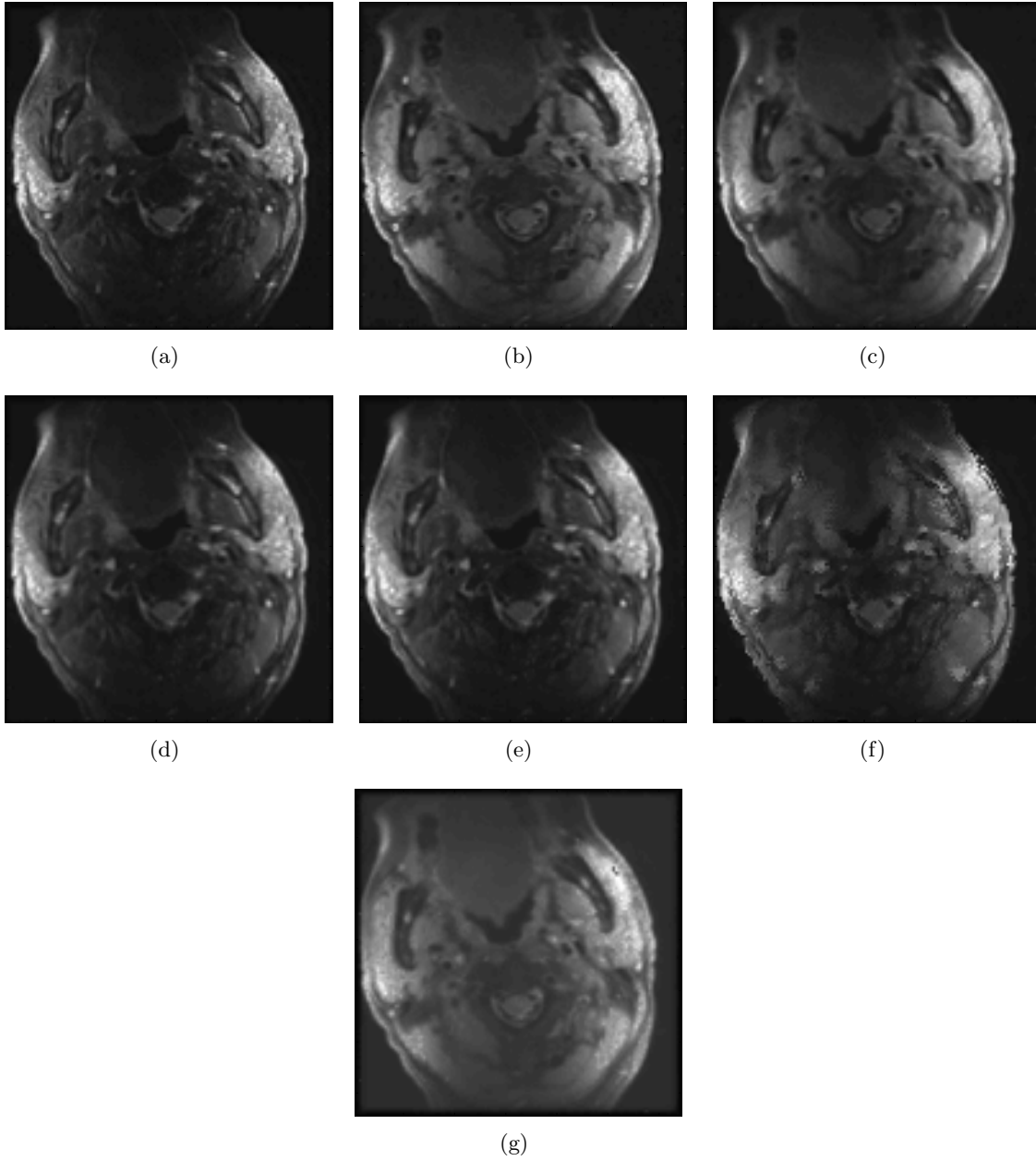


Figure 13. Comparison on VIII: (a) floating image $T(\cdot)$; (b) target image $D(\cdot)$; (c) $T \circ \tilde{\varphi}_N(\cdot)$ in Algorithm 4.1, $\text{Re.SSD}=5.28\%$; (d) 1DFDIM, $\text{Re.SSD}=76.09\%$; (e) DFIRA, $\text{Re.SSD}=66.54\%$; (f) LDDMM, $\text{Re.SSD}=51.23\%$; (g) FBNE, $\text{Re.SSD}=24.41\%$.

776 on the original variational model. However, under the framework of the Nash game theory,
 777 the final solution may be not the solution of the original variational model. This raises the
 778 uncertainty of the solution. In this paper, the proposed model (1.3) and related multiscale
 779 approach (2.1)-(2.2), aim at minimizing the similarity $S_{lc}(\mathbf{u}, m, s)$ on some smooth set $\mathcal{L}(\Omega)$,
 780 and achieves the solution of the greedy problem which joints image registration and intensity

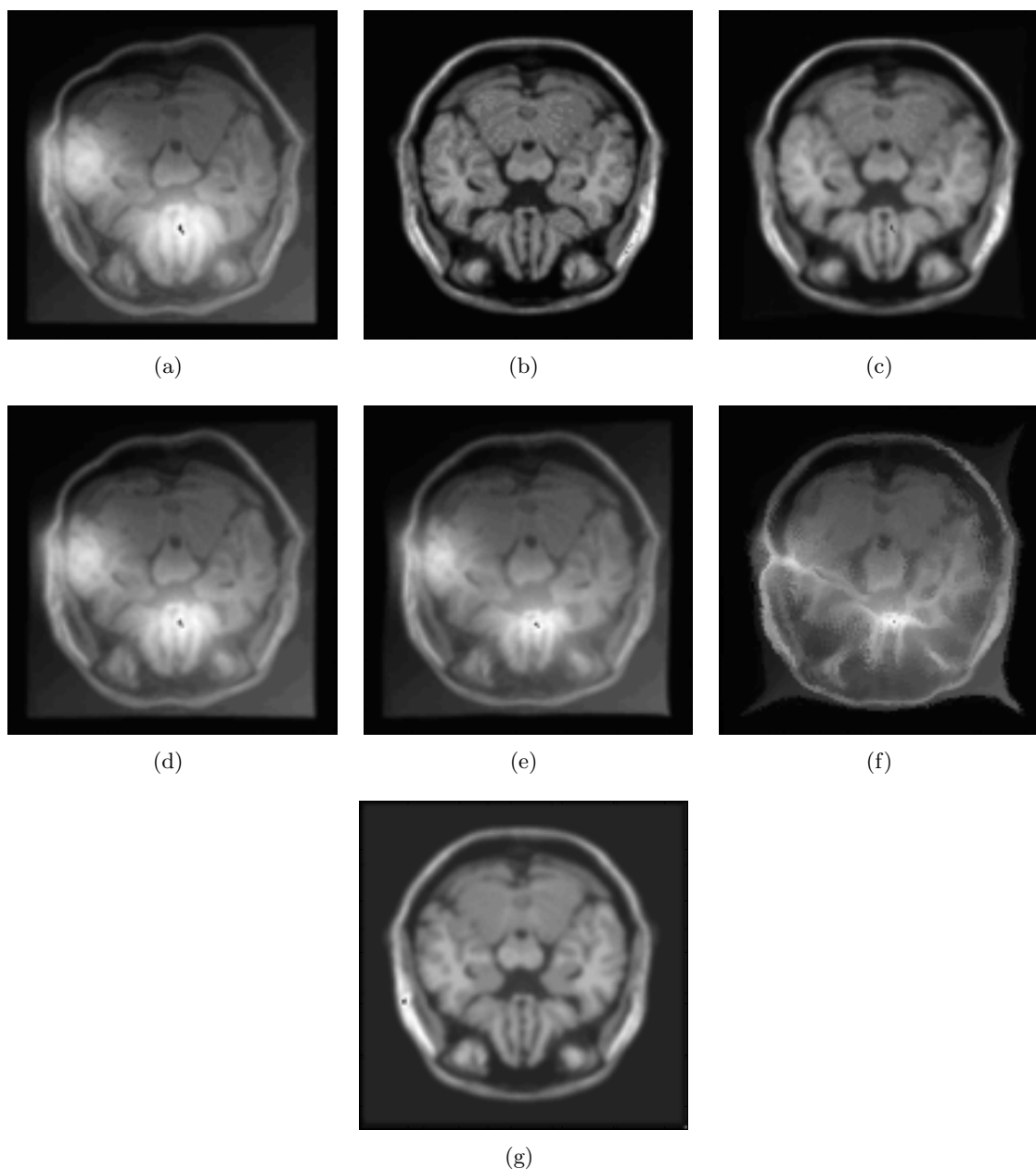


Figure 14. Comparison on IX: (a) floating image $T(\cdot)$; (b) target image $D(\cdot)$; (c) $T \circ \varphi_N(\cdot)$ in Algorithm 4.1, Re_SSD=3.05%; (d) 1DFDIM, Re_SSD=83.2%; (e) DFIRA, Re_SSD=68.96%; (f) LDDMM, Re_SSD=36.18%; (g) FBNE, Re_SSD=15.44%.

781 correction. This is also the reason why the proposed model achieves a better result than
 782 FBNE (see Fig 12-Fig 14 and Table 3).

783 **6.2. Limitation.** Although the proposed multiscale approach is capable of handling chal-
 784 lenging image registration task such as large deformation and intensity inhomogeneity, we face

785 the difficulties in scenario of occlusion or blur, see Fig 15-Fig 16 for details. The failure of Fig
 786 15-Fig 16 may be due to the nonlocal intensity inhomogeneity of occlusion or blur (Note the
 787 bias introduced in this paper is only capable of characterizing local intensity inhomogeneity).
 788 To address this challenge, some nonlocal methods are necessary to be introduced in image reg-
 789 istration, for example, registration joint blind deblurring [26], registration joint inpainting [37].
 790 These may be new topics in registration with nonlocal intensity inhomogeneity.

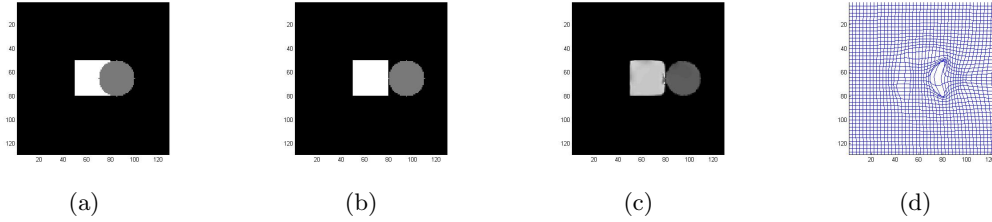


Figure 15. Registration on occlusion: (a) floating image $T(\cdot)$; (b) target image $D(\cdot)$; (c) registration $T_c \circ \varphi_N(\cdot)$; (d) deformation.

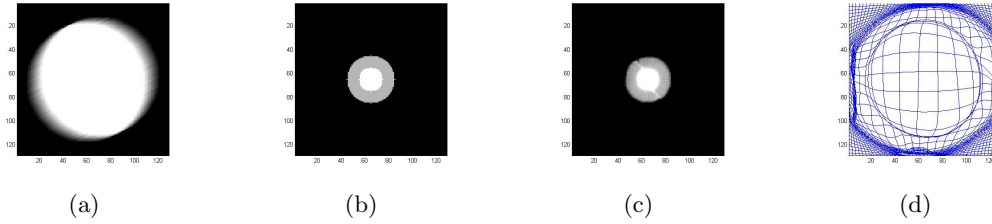


Figure 16. Registration on blur: (a) floating image $T(\cdot)$; (b) target image $D(\cdot)$; (c) registration $T_c \circ \varphi_N(\cdot)$; (d) deformation.

791 **7. Conclusion.** In this paper, we propose a variational model for joint diffeomorphic im-
 792 age registration and intensity correction. Based on the joint model, a related greedy matching
 793 problem (2.17) is proposed. For solving the greedy matching problem (2.17), a multiscale
 794 approach is introduced to addresses the instability by directly solving the greedy matching
 795 problem (2.17), which provides a theoretical support for this kind of research. For the numeri-
 796 cal computation of the multiscale approach, an ADM method is proposed and the convergence
 797 of this process is proved. In addition, a coarse-to-fine strategy is further introduced to acceler-
 798 ate the registration algorithm and its convergence is also established. Finally, three different
 799 kinds of numerical tests are performed to validate the theoretical results. For the future
 800 research, we may extend this work to the field of joint image registration and segmentation.

801 **Acknowledgments.** The authors of this paper would like to thank Hang Li in Hospital of
 802 Stomatology, Wuhan University, for providing the data for Test II. Thanks also to the referees
 803 for their very helpful remarks.

804

REFERENCES

- 805 [1] M. BURGER, J. MODERSITZKI, AND L. RUTHOTTO, *A hyperelastic regularization energy for image regis-*
806 *tration*, SIAM J. Sci. Comput., 35(1) (2013), pp. 132–148, <https://doi.org/10.1137/110835955>.
- 807 [2] A. CHAMBOLLE, *An algorithm for total variation minimization and applications*, J. Math. Imaging Vis.,
808 20 (2004), pp. 89–97, <https://doi.org/10.1023/B:JMIV.0000011325.36760.1e>.
- 809 [3] C. CHEN AND O. OKTEM, *Indirect image registration with large diffeomorphic deformations*, SIAM J.
810 Imaging Sci., 11 (2018), pp. 575–617, <https://doi.org/10.1137/17M1134627>.
- 811 [4] Y. CHEN, J. SHI, M. RAO, AND J. LEE, *Deformable multi-modal image registration by maximizing rnyi’s*
812 *statistical dependence measure*, Inverse Probl. Imaging, 9(1) (2015), pp. 79–103, <https://doi.org/10.3934/ipi.2015.9.79>.
- 813 [5] G. CHRISTENSEN, R. RABBITT, AND M. MILLER, *Deformable templates using large deformation kinemat-*
814 *ics*, IEEE Trans. Image Process., 5(10) (1996), pp. 1435–1447, <https://doi.org/10.1109/83.536892>.
- 815 [6] N. CHUMCHOB, *Vectorial total variation-based regularization for variational image registration*, IEEE
816 Trans. Image Process., 22(11) (2013), pp. 4551–4559, <https://doi.org/10.1109/TIP.2013.2274749>.
- 817 [7] N. CHUMCHOB, K. CHEN, AND C. LOEZA, *A fourth-order variational image registration model and its*
818 *fast multi grid algorithm*, Multiscale Model. Simul., 9(1) (2011), pp. 89–128, [https://doi.org/10.1137/](https://doi.org/10.1137/100788239)
819 [100788239](https://doi.org/10.1137/100788239).
- 820 [8] L. K. CHUN AND L. M. LUI, *Landmark and intensity based registration with large deformations via*
821 *quasi-conformal maps*, SIAM J. Imaging Sci., 7(4) (2013), pp. 2364–2392, [https://doi.org/10.1137/](https://doi.org/10.1137/130943406)
822 [130943406](https://doi.org/10.1137/130943406).
- 823 [9] N. DEBROUX, C. LE GUYADER, AND L. VESE, *A multiscale deformation representation*, SIAM J. Imaging
824 Sci., 16(2) (2023), pp. 802–841, <https://doi.org/10.1137/22M151020>.
- 825 [10] F. DEMENGEL, G. DEMENGEL, AND R. ERNE, *Functional spaces for the theory of elliptic partial differ-*
826 *ential equations*, Springer London, 2012.
- 827 [11] M. DROSKE AND M. RUMPF, *A variational approach to nonrigid morphological image registration*, SIAM
828 J. Appl. Math., 64(2) (2004), pp. 668–687, <https://doi.org/10.2307/4096004>.
- 829 [12] M. EBRAHIMI AND S. KULASEHARAN, *Deformable image registration and intensity correction of cardiac*
830 *perfusion mri*, Statistical Atlases and Computational Models of the Heart - Imaging and Modelling
831 Challenges, 8896 (2015), pp. 13–20, https://doi.org/10.1007/978-3-319-14678-2_2.
- 832 [13] M. EBRAHIMI, A. LAUSCH, AND A. L. MARTEL, *A gauss-newton approach to joint image registration and*
833 *intensity correction*, Computer Methods and Programs in Biomedicine, 112(3) (2013), pp. 398–406,
834 <https://doi.org/10.1016/j.cmpb.2013.07.026>.
- 835 [14] L. EVANS, *Partial differential equations*, American Mathematical Society, 2010.
- 836 [15] D. FERREIRA, E. RIBEIRO, AND C. BARCELOS, *A variational approach to non-rigid image registration*
837 *with bregman divergences and multiple features*, Pattern Recognition, 77 (2018), pp. 237–247, <https://doi.org/10.1016/j.patcog.2017.12.015>.
- 838 [16] E. HABER AND J. MODERSITZKI, *A multilevel method for image registration*, SIAM J. Sci. Comput., 27(5)
839 (2006), pp. 1594–1607, <https://doi.org/10.1137/040608106>.
- 840 [17] H. HAN, *A variational model with fractional-order regularization term arising in registration of diffusion*
841 *tensor image*, Inverse Probl. Imaging, 12(6) (2018), pp. 1263–1291, [https://doi.org/aimsciences.org/](https://doi.org/aimsciences.org/article/doi/10.3934/ipi.2018053)
842 [/article/doi/10.3934/ipi.2018053](https://doi.org/aimsciences.org/article/doi/10.3934/ipi.2018053).
- 843 [18] H. HAN AND A. WANG, *A fast multi grid algorithm for 2D diffeomorphic image registration model*, J.
844 Comput. Appl. Math., 394 (2021), p. 113567, <https://doi.org/10.1016/j.cam.2021.113576>.
- 845 [19] H. HAN AND Z. WANG, *A diffeomorphic image registration model with fractional-order regularization and*
846 *Cauchy-Riemann constraint*, SIAM J. Imaging Sci., 13 (2020), pp. 1240–1271, <https://doi.org/10.1137/19M1260621>.
- 847 [20] H. HAN AND Z. WANG, *3D diffeomorphic image registration with cauchy-riemann constraint and lower*
848 *bounded deformation divergence*, ESAIM Math. Model. Num., 57(1) (2023), pp. 299–328, [https://doi.](https://doi.org/10.1051/m2an/2022080)
849 [org/10.1051/m2an/2022080](https://doi.org/10.1051/m2an/2022080).
- 850 [21] H. HAN, Z. WANG, AND Y. ZHANG, *Multiscale approach for two-dimensional diffeomorphic image regis-*
851 *tration*, Multiscale Model. Simul., 19(4) (2021), pp. 1538–1572, <https://doi.org/10.1137/20M1383987>.
- 852 [22] H. HAN, Z. WANG, AND Y. ZHANG, *Multiscale approach for three-dimensional conformal image registra-*
853 *tion*, SIAM J. Imaging Sci., 15(3) (2022), pp. 1431–1468, <https://doi.org/10.1137/21M1455929>.
- 854 [23] C. KANZOW AND Y. SHEHU, *Strong convergence of a double projection-type method for monotone*
855 *variational inequalities in hilbert spaces*, J. Fixed Point Theory Appl., 20 (1) (2018), pp. 51–72,
856
857
858

- 859 <https://doi.org/doi.org/10.1007/s11784-018-0531-8>.
- 860 [24] H. LI, W. GUO, J. LIU, L. CUI, AND D. XIE, *Image segmentation with adaptive spatial priors from*
861 *joint registration*, SIAM J. Imaging Sci., 15(3) (2022), pp. 1314–1344, [https://doi.org/10.1137/](https://doi.org/10.1137/21M1444874)
862 [21M1444874](https://doi.org/10.1137/21M1444874).
- 863 [25] J. LI, Y. SHI, G. TRAN, I. DINOVI, D. WANG, AND A. TOGA, *Fast local trust region for diffusion tensor*
864 *registration using exact reorientation and regularization*, IEEE Trans Med Imaging, 33(5) (2014),
865 pp. 1–43, <https://doi.org/10.1109/TMI.2013.2274051>.
- 866 [26] J. LIU, M. YAN, AND T. ZENG, *Surface-aware blind image deblurring*, IEEE Trans. Pattern Anal. Mach.
867 Intell, 43(2) (2021), pp. 1041–1055, <https://doi.org/10.1109/TPAMI.2019.2941472>.
- 868 [27] L. M. LUI AND T. C. NG, *A splitting method for diffeomorphism optimization problem using beltrami*
869 *coefficients*, J. Sci. Comput., 63 (2015), pp. 573–611, <https://doi.org/10.1007/s10915-014-9903-4>.
- 870 [28] F. MAES, A. COLLIGNON, D. VANDERMEULEN, G. MARCHAL, AND P. SUETENS, *Diffeomorphic demons:*
871 *Efficient non-parametric image registration*, IEEE Trans. Med. Imaging., 16(2) (1997), pp. 187–198,
872 <https://doi.org/10.1109/42.563664>.
- 873 [29] K. MALEELAI, C. WATCHARARUANGWIT, AND N. CHUMCHOB, *An improved numerical method for vari-*
874 *ational image registration model with intensity correction*, Journal of Interdisciplinary Mathematics,
875 25(4) (2022), pp. 1005–1022, <https://doi.org/10.1080/09720502.2021.1889781>.
- 876 [30] D. QIU, K. C. LAM, AND L. M. LUI, *Computing quasiconformal folds*, SIAM J. Imaging Sci., 12(3)
877 (2019), pp. 1392–1424, <https://doi.org/10.1137/18M1220042>.
- 878 [31] D. QIU AND L. M. LUI, *Inconsistent surface registration via optimization of mapping distortions*, J. Sci.
879 Comput., 83 (2020), pp. 1–31, <https://doi.org/10.1007/s10915-020-01246-5>.
- 880 [32] E. TADMOR AND L. V. S. NEZZAR, *A multiscale image representation using hierarchical (bv, l²) decom-*
881 *positions*, Multiscale Model. Simul., 2 (2004), pp. 554–579, <https://doi.org/10.1137/030600448>.
- 882 [33] A. THELJANI AND K. CHEN, *A nash game based variational model for joint image intensity correction*
883 *and registration to deal with varying illumination*, Inverse Probl., 36 (2020), p. 034002, [https://doi.](https://doi.org/10.1088/1361-6420/ab2934)
884 [org/10.1088/1361-6420/ab2934](https://doi.org/10.1088/1361-6420/ab2934).
- 885 [34] T. VERCAUTEREN, X. PENNECB, A. PERCHANTA, AND N. AYACHEB, *Diffeomorphic demons:efficient*
886 *non-parametric image registration*, Neuroimage, 45(1) (2009), pp. 61–72, [https://doi.org/10.1109/](https://doi.org/10.1109/TMI.2016.2610583)
887 [TMI.2016.2610583](https://doi.org/10.1109/TMI.2016.2610583).
- 888 [35] R. XU, P. ATHAVALE, A. NACHMAN, AND G. A. WRIGHT, *Multiscale registration of real-time and prior*
889 *mri data for image-guided cardiac interventions*, IEEE Trans. Bio-Med. Eng., 61(10) (2014), pp. 2621–
890 2632, <https://doi.org/10.1109/TBME.2014.2324998>.
- 891 [36] C. P. YUNG, G. CHOI, K. CHEN, AND L. M. LUI, *Efficient feature-based image registration by mapping*
892 *sparsified surfaces*, J. Vis. Commun. Image R., 55 (2018), pp. 561–571, [https://doi.org/10.1016/j.](https://doi.org/10.1016/j.jvcir.2018.07.005)
893 [jvcir.2018.07.005](https://doi.org/10.1016/j.jvcir.2018.07.005).
- 894 [37] C. ZHANG, W. YANG, X. LI, AND H. HAN, *MMGInpainting: Multi-modality guided image inpainting*
895 *based on diffusion models*, IEEE Trans. Multimedia, 1 (2024), p. accepted, [https://doi.org/10.1109/](https://doi.org/10.1109/TMM.2024.3382484)
896 [TMM.2024.3382484](https://doi.org/10.1109/TMM.2024.3382484).
- 897 [38] D. ZHANG AND K. CHEN, *A novel diffeomorphic model for image registration and its algorithm*, J. Math.
898 Imaging Vision, 2018 (2018), pp. 1–30, <https://doi.org/10.1007/s10851-018-0811-3>.
- 899 [39] D. ZHANG AND K. CHEN, *3D orientation-preserving variational models for accurate image registration*,
900 SIAM J. Imaging Sci., 13(3) (2020), pp. 1653–1691, <https://doi.org/10.1137/20M1320006>.
- 901 [40] D. ZHANG, G. P. T. CHOI, J. ZHANG, AND L. M. LUI, *A unifying framework for n-dimensional quasi-*
902 *conformal mappings*, SIAM J. Imaging Sci., 15(2) (2022), pp. 960–988, [https://doi.org/10.1137/](https://doi.org/10.1137/21M1457497)
903 [21M1457497](https://doi.org/10.1137/21M1457497).
- 904 [41] J. ZHANG AND K. CHEN, *Variational image registration by a total fractional-order variation model*, J.
905 Comput. Phys., 293 (2015), pp. 442–461, <https://doi.org/10.1016/j.jcp.2015.02.021>.
- 906 [42] J. ZHANG, K. CHEN, AND B. YU, *A novel high-order functional based image registration model with*
907 *inequality constraint*, Comput. Math. Appl., 72(12) (2014), pp. 2887–2899, [https://doi.org/10.1016/](https://doi.org/10.1016/j.camwa.2016.10.018)
908 [j.camwa.2016.10.018](https://doi.org/10.1016/j.camwa.2016.10.018).

909 **Appendix A. Estimation on the L^∞ norm for the Hessian matrix of $\ln(T \circ \tilde{\varphi}_{n-1}(\mathbf{x} +$
910 $\mathbf{v}_n^k) - s_{n-1} - \delta s_n^k$ with respect to \mathbf{v}_n^k .**

911 The Hessian matrix of $\ln(T \circ \tilde{\varphi}_{n-1}(\mathbf{x} + \mathbf{v}_n^k) - s_{n-1} - \delta s_n^k)$ is formulated as

$$912 \quad H = \frac{1}{(T \circ \tilde{\varphi}_{n-1}(\mathbf{x} + \mathbf{v}_n^k) - s_{n-1} - \delta s_n^k)^2} \begin{pmatrix} H_1 & H_2 \\ H_2 & H_3 \end{pmatrix},$$

913 where $H_1 = T \circ \tilde{\varphi}_{n-1}(\mathbf{x} + \mathbf{v}_n^k) \frac{\partial^2}{\partial x_1^2} (T \circ \tilde{\varphi}_{n-1}(\mathbf{x} + \mathbf{v}_n^k)) - \left(\frac{\partial}{\partial x_1} T \circ \tilde{\varphi}_{n-1}(\mathbf{x} + \mathbf{v}_n^k) \right)^2$, $H_2 = T \circ$
 914 $\tilde{\varphi}_{n-1}(\mathbf{x} + \mathbf{v}_n^k) \frac{\partial^2}{\partial x_1 \partial x_2} (T \circ \tilde{\varphi}_{n-1}(\mathbf{x} + \mathbf{v}_n^k)) - \left(\frac{\partial}{\partial x_1} T \circ \tilde{\varphi}_{n-1}(\mathbf{x} + \mathbf{v}_n^k) \right) \left(\frac{\partial}{\partial x_2} T \circ \tilde{\varphi}_{n-1}(\mathbf{x} + \mathbf{v}_n^k) \right)$ and
 915 $H_3 = T \circ \tilde{\varphi}_{n-1}(\mathbf{x} + \mathbf{v}_n^k) \frac{\partial^2}{\partial x_2^2} (T \circ \tilde{\varphi}_{n-1}(\mathbf{x} + \mathbf{v}_n^k)) - \left(\frac{\partial}{\partial x_2} T \circ \tilde{\varphi}_{n-1}(\mathbf{x} + \mathbf{v}_n^k) \right)^2$. By (1.3) and (3.6),
 916 we know $(T \circ \tilde{\varphi}_{n-1}(\mathbf{x} + \mathbf{v}_n^k) - s_{n-1} - \delta s_n^k)^2 \geq (\kappa - \kappa_0)^2$.

917 Now we give an estimate on the L^∞ norm of H_1 . Since $\alpha > 3$, by the Sobolev embdding
 918 Theorem [10] ($H_0^\alpha(\Omega) \hookrightarrow C^2(\Omega)$), we obtain

$$919 \quad \begin{aligned} \|\nabla^2 \varphi\|_{C(\Omega)}^2 &= \|\nabla^2 \mathbf{u}\|_{C(\Omega)}^2 \leq CR_1(\mathbf{u}) \leq C\lambda_n \int_{\Omega} (m_{n-1} + \ln D - \ln(T \circ \tilde{\varphi}_{n-1} - s_{n-1}))^2 d\mathbf{x} \\ &\leq 2C\lambda_n |\Omega| (K^2 + \ln^2(\bar{M}/\kappa)^2) \leq \lambda_n \tilde{M}, \end{aligned}$$

920 where $\tilde{M} \triangleq \tilde{M}(\Omega, \alpha) = 2C|\Omega|(K^2 + \ln^2(\bar{M}/\kappa)^2) > 0$ and $C = C(\Omega, \alpha)$ is a positive constant
 921 (see Lemma 3.2 and Lemma 3.3 in [17] for details). Similarly, there holds

$$922 \quad \|\mathbf{u}_n\|_{C^1(\Omega)}^2 \leq \lambda_n \tilde{M}.$$

923 Note that

$$924 \quad (\text{A.1}) \quad \nabla_{\mathbf{x}} \tilde{\varphi}_n(\mathbf{x}) = \nabla_{\mathbf{g}_1} \varphi_0 \cdot \nabla_{\mathbf{g}_2} \varphi_1 \cdots \nabla_{\mathbf{g}_{n-1}} \varphi_{n-2} \cdot \nabla_{\mathbf{g}_n} \varphi_{n-1} \cdot \nabla_{\mathbf{x}} \varphi_n(\mathbf{x}),$$

925 where $\mathbf{g}_k = \varphi_k \circ \varphi_2 \cdots \varphi_n$ for $k = 1, 2, \dots, n$. Since \mathbf{g}_k are mappings from Ω to Ω , by (A.1),
 926 we obtain

$$927 \quad \|\nabla_{\mathbf{x}} \tilde{\varphi}_n(\mathbf{x})\|_{C(\Omega)}^2 \leq \lambda_0 \lambda_1 \cdots \lambda_n \tilde{M}^n \leq (\lambda_n \tilde{M})^n.$$

928 Then by the chain rule, we have

$$929 \quad \frac{\partial T \circ \tilde{\varphi}_{n-1}}{\partial x_1} = \frac{\partial T \circ \tilde{\varphi}_{n-1}}{\partial \tilde{\varphi}_{n-1}^1} \frac{\partial \tilde{\varphi}_{n-1}^1}{\partial x_1} + \frac{\partial T \circ \tilde{\varphi}_{n-1}}{\partial \tilde{\varphi}_{n-1}^2} \frac{\partial \tilde{\varphi}_{n-1}^2}{\partial x_1}$$

930 and

$$931 \quad \begin{aligned} \frac{\partial^2 T \circ \tilde{\varphi}_{n-1}}{\partial x_1^2} &= \frac{\partial^2 T \circ \tilde{\varphi}_{n-1}}{\partial (\varphi_{n-1}^1)^2} \left(\frac{\partial \varphi_{n-1}^1}{\partial x_1} \right)^2 + 2 \frac{\partial^2 T \circ \tilde{\varphi}_{n-1}}{\partial \varphi_{n-1}^1 \partial \varphi_{n-1}^2} \frac{\partial \tilde{\varphi}_{n-1}^1}{\partial x_1} \frac{\partial \tilde{\varphi}_{n-1}^2}{\partial x_1}, \\ &+ \frac{\partial T \circ \tilde{\varphi}_{n-1}}{\partial \tilde{\varphi}_{n-1}^2} \frac{\partial^2 \tilde{\varphi}_{n-1}^2}{\partial x_1^2} + \frac{\partial^2 T \circ \tilde{\varphi}_{n-1}}{\partial (\varphi_{n-1}^2)^2} \left(\frac{\partial \varphi_{n-1}^2}{\partial x_1} \right)^2 \\ &+ \frac{\partial T \circ \tilde{\varphi}_{n-1}}{\partial \tilde{\varphi}_{n-1}^1} \frac{\partial^2 \tilde{\varphi}_{n-1}^1}{\partial x_1^2} + \frac{\partial T \circ \tilde{\varphi}_{n-1}}{\partial \tilde{\varphi}_{n-1}^2} \frac{\partial^2 \tilde{\varphi}_{n-1}^2}{\partial x_1^2}. \end{aligned}$$

932 This concludes

$$933 \quad \left\| \frac{\partial T \circ \tilde{\varphi}_{n-1}}{\partial x_1} \right\|_{C(\Omega)}^2 \leq 4\overline{M}(\lambda_n \widetilde{M})^n$$

934 and

$$935 \quad \left\| \frac{\partial^2 T \circ \tilde{\varphi}_{n-1}}{\partial x_1^2} \right\|_{C(\Omega)}^2 \leq 6\overline{M}(\lambda_n \widetilde{M})^n.$$

936 Based on the above mentioned discussion, we can get

$$937 \quad \|H_1\|_{C(\Omega)} \leq 10\overline{M}^2(\lambda_n \widetilde{M})^n.$$

938 In addition, we can also obtain the similar estimate for H_2, H_3 . Therefore, we conclude

$$939 \quad \|H(\sigma)\|_{C(\Omega)} \leq \frac{10\overline{M}^2(\lambda_n \widetilde{M})^n}{(\kappa - \kappa_0)^2}.$$

940 **Appendix B. Multigrid method for PDE (3.28).** By adopting Grunwald approximation
941 [41], $\frac{\partial^\alpha f(\mathbf{x})}{\partial x_i^\alpha}, \frac{\partial^{\alpha^*} f(\mathbf{x})}{\partial x_i^{\alpha^*}} (i = 1, 2)$ are discretized as follows:

$$942 \quad (\text{B.1}) \quad \frac{\partial^\alpha f(\mathbf{x}_{p,q})}{\partial x_i^\alpha} = \delta_{i-}^\alpha f(\mathbf{x}_{p,q}) + O(h), \quad \frac{\partial^{\alpha^*} f(\mathbf{x}_{p,q})}{\partial x_i^{\alpha^*}} = \delta_{i+}^{\alpha^*} f(\mathbf{x}_{p,q}) + O(h),$$

944 where $\delta_{1-}^\alpha f_{p,q} = \frac{1}{h^\alpha} \sum_{l=0}^{p+1} \rho_l^{(\alpha)} f_{p-l+1,q}$, $\delta_{1+}^{\alpha^*} f_{p,q} = \frac{1}{h^\alpha} \sum_{l=0}^{N-p+2} \rho_l^{(\alpha)} f_{p+l-1,q}$, $\delta_{2-}^\alpha f_{p,q} = \frac{1}{h^\alpha} \sum_{m=0}^{q+1} \rho_m^{(\alpha)}$
945 $f_{p,q-m+1}$, $\delta_{2+}^{\alpha^*} f_{p,q,r} = \frac{1}{h^\alpha} \sum_{m=0}^{N-q+2} \rho_m^{(\alpha)} f_{p,q+m-1}$, and $\rho_l^{(\alpha)}$ is computed by the formula $\rho_0^{(\alpha)} = 1$,
946 $\rho_l^{(\alpha)} = (1 - \frac{1+\alpha}{l})\rho_{l-1}^{(\alpha)}$. Note that here, we use $f_{p,q}$ to denote $f(\mathbf{x}_{p,q})$ for any function f .

947 Let $U_q = (f_{1,q}, f_{2,q}, \dots, f_{N,q})^T$, then it follows from (B.1) that

$$948 \quad \frac{\partial^\alpha U_q}{\partial x_1^\alpha} \approx B_{N,\alpha} U_q, \quad \frac{\partial^{\alpha^*} U_q}{\partial x_1^{\alpha^*}} \approx B_{N,\alpha}^T U_q,$$

949 where $\frac{\partial^\alpha U_q}{\partial x_1^\alpha} = \left(\frac{\partial^\alpha f_{1,q}}{\partial x_1^\alpha}, \frac{\partial^\alpha f_{2,q}}{\partial x_1^\alpha}, \dots, \frac{\partial^\alpha f_{N,q}}{\partial x_1^\alpha} \right)^T$, $\frac{\partial^{\alpha^*} U_q}{\partial x_1^{\alpha^*}} = \left(\frac{\partial^{\alpha^*} f_{1,q}}{\partial x_1^{\alpha^*}}, \frac{\partial^{\alpha^*} f_{2,q}}{\partial x_1^{\alpha^*}}, \dots, \frac{\partial^{\alpha^*} f_{N,q}}{\partial x_1^{\alpha^*}} \right)^T$ and

$$950 \quad B_{N,\alpha} = \frac{1}{h^\alpha} \begin{pmatrix} \rho_1^{(\alpha)} & \rho_0^{(\alpha)} & 0 & \cdots & 0 & 0 \\ \rho_2^{(\alpha)} & \rho_1^{(\alpha)} & \rho_0^{(\alpha)} & \cdots & 0 & 0 \\ \vdots & \vdots & \vdots & \ddots & \vdots & \vdots \\ \rho_{N-1}^{(\alpha)} & \rho_{N-2}^{(\alpha)} & \rho_{N-3}^{(\alpha)} & \cdots & \rho_1^{(\alpha)} & \rho_0^{(\alpha)} \\ \rho_N^{(\alpha)} & \rho_{N-1}^{(\alpha)} & \rho_{N-2}^{(\alpha)} & \cdots & \rho_2^{(\alpha)} & \rho_1^{(\alpha)} \end{pmatrix}.$$

952 Hence, we obtain

$$953 \quad \frac{\partial^{\alpha^*}}{\partial x_1^{\alpha^*}} \left(\frac{\partial^\alpha U_q}{\partial x_1^\alpha} \right) = B_{N,\alpha}^T B_{N,\alpha} U_q \triangleq A_{N,\alpha} U_q.$$

954 In a similar way, we obtain the following two approximations for $\frac{\partial^{\alpha^*}}{\partial x_2^{\alpha^*}} \left(\frac{\partial^\alpha f(\mathbf{x})}{\partial x_2^\alpha} \right)$,

$$955 \quad \frac{\partial^{\alpha^*}}{\partial x_2^{\alpha^*}} \left(\frac{\partial^\alpha V_p}{\partial x_2^\alpha} \right) = A_{N,\alpha} V_p,$$

956 where $V_p = (f_{p,1}, f_{p,2}, \dots, f_{p,N})^T$. By adopting the Grunwald approximation, $\text{div}^{\alpha^*}(\nabla^\alpha \mathbf{u}_n^{k+1})$
 957 and $\Delta \mathbf{u}_n^{k+1}$ are approximated by the following two formulas

$$958 \quad (\text{B.2}) \quad \left(\text{div}^{\alpha^*}(\nabla^\alpha u_{n,\beta}^{k+1}) \right)_{p,q} \approx \sum_{l=0}^N \left(a_{N,\alpha}(p,l)(u_{n,\beta}^{k+1})_{l,q} + a_{N,\alpha}(q,l)(u_{n,\beta}^{k+1})_{p,l} \right)$$

959 and

$$960 \quad (\text{B.3}) \quad \left(\Delta u_{n,\beta}^{k+1} \right)_{p,q} \approx \frac{1}{h^2} \left((u_{n,\beta}^{k+1})_{p+1,q} + (u_{n,\beta}^{k+1})_{p-1,q} + (u_{n,\beta}^{k+1})_{p,q+1} + (u_{n,\beta}^{k+1})_{p,q-1} - 4(u_{n,\beta}^{k+1})_{p,q} \right),$$

961 where $\beta = 1, 2$ and $a_{N,\alpha}(p, l)$ is the entry of matrix $A_{N,\alpha}$ at the intersection of p th row and
 962 l th column.

963 Then based on (B.2) and (B.3), (3.28) is discretized as follows

$$964 \quad (\text{B.4}) \quad \begin{aligned} & (1 + 4\gamma_n + 2\theta_n \mu (a_{N,\alpha}(p,p) + a_{N,\alpha}(q,q))) (u_{n,\beta}^{k+1})_{p,q} \\ & + 2\theta_n \mu \sum_{l=1, l \neq p,q}^{N_S} \left(a_{N,\alpha}(p,l)(u_{n,\beta}^{k+1})_{l,q} + a_{N,\alpha}(q,l)(u_{n,\beta}^{k+1})_{p,l} \right) \\ & - \gamma_n \left((u_{n,\beta}^{k+1})_{p+1,q} + (u_{n,\beta}^{k+1})_{p-1,q} + (u_{n,\beta}^{k+1})_{p,q+1} + (u_{n,\beta}^{k+1})_{p,q-1} \right) = (v_{n,\beta}^{k+1})_{p,q}, \end{aligned}$$

965 where $\gamma_n = \frac{2\theta_n \Theta}{h^2}$. Further, (B.4) induces the following solver for (3.28),

$$966 \quad (\text{B.5}) \quad \begin{aligned} (u_{n,\beta}^{k+1})_{p,q}^{(t+1)} &= \frac{1}{\Upsilon_n} \left((v_{n,\beta}^{k+1})_{p,q} - 2\theta_n \mu \sum_{l=1, l \neq p,q}^{N_S} \left(a_{N,\alpha}(p,l)(u_{n,\beta}^{k+1})_{l,q}^{(t)} + a_{N,\alpha}(q,l)(u_{n,\beta}^{k+1})_{p,l}^{(t)} \right) \right. \\ & \left. + \gamma_n \left((u_{n,\beta}^{k+1})_{p+1,q}^{(t)} + (u_{n,\beta}^{k+1})_{p-1,q}^{(t)} + (u_{n,\beta}^{k+1})_{p,q+1}^{(t)} + (u_{n,\beta}^{k+1})_{p,q-1}^{(t)} \right) \right), \end{aligned}$$

967 where $\Upsilon_n = 1 + 4\gamma_n + 2\theta_n \mu (a_{N,\alpha}(p,p) + a_{N,\alpha}(q,q))$ and $t = 0, 1, 2, \dots$.

968 To solve the algebraic system (B.4), many numerical techniques can be used, such as
 969 the Jacobi iteration, the Gauss-Siedel iteration and the multigrid method. Here we choose
 970 the multigrid method to accelerate the Jacobi iterative technique. One round of V-cycle of
 971 the multigrid method contains four steps: Step 1. Smoothing; Step 2. Restriction; Step 3.
 972 Coarsest grid solution; Step 4. Interpolation. Since this technique is similar to the steps
 973 in [18, 21], we omit the introduction for these four steps and refer the reader to [18, 21] for
 974 details. However, to make our paper self-contained, based on (B.5), the multigrid algorithm
 975 for (3.28) can be summarized in Algorithm B.1.

Algorithm B.1 2D multigrid algorithm for \mathbf{u} -problem

Initialization: $\mathbf{u}_n^{k+1,h} = \mathbf{u}_n^{k,h}$, $\mathbf{u}_{n,0}^{k+1,h} = \mathbf{u}_n^{k,h} + \mathbf{\Pi}$, $\mu > 0$, $\bar{k} = 0$ and maximum iteration times K .

while $\|\mathbf{u}_n^{k+1,h} - \mathbf{u}_{n,0}^{k+1,h}\| \geq \|\mathbf{\Pi}\|$ and $\bar{k} \leq K$ **do**

$\mathbf{u}_{n,0}^{k+1,h} = \mathbf{u}_n^{k+1,h}$.

Step 1. relax (B.5) with initial guess $\mathbf{u}_n^{k+1,h}$; compute residual error $\mathbf{r}_n^{k+1,h}$ on Ω^h ;

Set $level = L$.

Step 2. restrict the residual error to Ω^H by using $\mathbf{r}_n^{k+1,H} = R_h^H \mathbf{r}_n^{k+1,h}$;

Set $level = level - 1$, $H = 2h$, and relax (B.5) by replacing \mathbf{v}_n^{k+1} with $\mathbf{r}_n^{k+1,H}$, and with initial guess $\mathbf{u}_n^{k+1,H} = \mathbf{0}$ to obtain approximations $\bar{\mathbf{u}}_n^{k+1,H}$; update residual error $\mathbf{r}_n^{k+1,H}$;

Step 3.

if $level = 1$,

do: accurately solve the system (B.5) by replacing \mathbf{v}_n^{k+1} with $\mathbf{r}_n^{k+1,H}$ to obtain the solution $\mathbf{u}_n^{k+1,H}$;

else

do: repeat **Step 2** until $level = 1$.

end if

Step 4.

if $level = L$,

do: relax (B.5) to obtain the final solution $\mathbf{u}_n^{k+1,h}$ for this round and let $\bar{k} = \bar{k} + 1$;

else

do(repeat): interpolate the correction to next fine grid by letting $\mathbf{u}_{n,t}^{k+1,h} = I_H^h \mathbf{u}_n^{k+1,H}$;

update current grid approximations using correction $\hat{\mathbf{u}}_n^{k+1,h} = \mathbf{u}_{n,t}^{k+1,h} + \bar{\mathbf{u}}_n^{k+1,h}$; relax (B.5)

with initial guess $\hat{\mathbf{u}}_n^{k+1,h}$ on fine grid to obtain approximations $\mathbf{u}_n^{k+1,h}$ and let $level = level + 1$. Repeat this process until $level = L$.

end if.

end while

Output: $\mathbf{u}_n^{k+1} = \mathbf{u}_n^{k+1,h}$.
